The Measurement of Solar Spectral Irradiances at Wavelengths between 40 and 4000 A.

Final Report for NASA Grant NSG 7559

March 1983

J. G. Timothy
Principal Investigator

Department of Astro-Geophysics
University of Colorado
Boulder, CO 80309

Contents

I. INTRODUCTION

Solar radiation at wavelengths below about 3100 A is totally absorbed by the terrestrial atmosphere and provides the dominate source of energy for heating, dissociation, and ionization. An accurate knowledge of the solar spectral irradiances at ultraviolet and soft x-ray wavelengths is accordingly of fundamental importance in studies of the photochemistry of the stratosphere, mesosphere and thermosphere, and of the energy balance of the ionosphere. In addition, a determination of the effects of specific solar features on the magnitudes of the solar spectral irradiances can provide fundamental insights into variations in the state of the plasma and in the magnetic field configurations in the outer solar atmosphere over the solar cycle. These data are crucial for an understanding of conditions in the atmospheres of the Sun and other cool stars. Unfortunately, because of the experimental difficulties, the available data are extremely limited and there are major uncertainties in many of the measurements. The magnitudes of the spectral irradiances have not yet been determined with sufficient accuracy and the effects of specific solar features on the variability of the spectral irradiances over the solar cycle have yet to be quantified.

Under the subject grant, we have refurbished and upgraded two 1/8-meter Ebert-Fastie spectrometers in order to measure the solar spectral irradiances between 1160 and 3100 A. Further, a novel, evacuated 1/4-meter normal-incidence spectrometer was fabricated for spectral irradiance measurements over the wavelength range from 1250 to 250 A. Procedures were developed for the calibration of all three instruments utilizing standards at the National Bureau of Standards (NBS). In addition, the procurement of a third 1/8-meter Ebert-Fastie spectrometer to cover the wavelength range from 2500 to 4000 A was initiated.

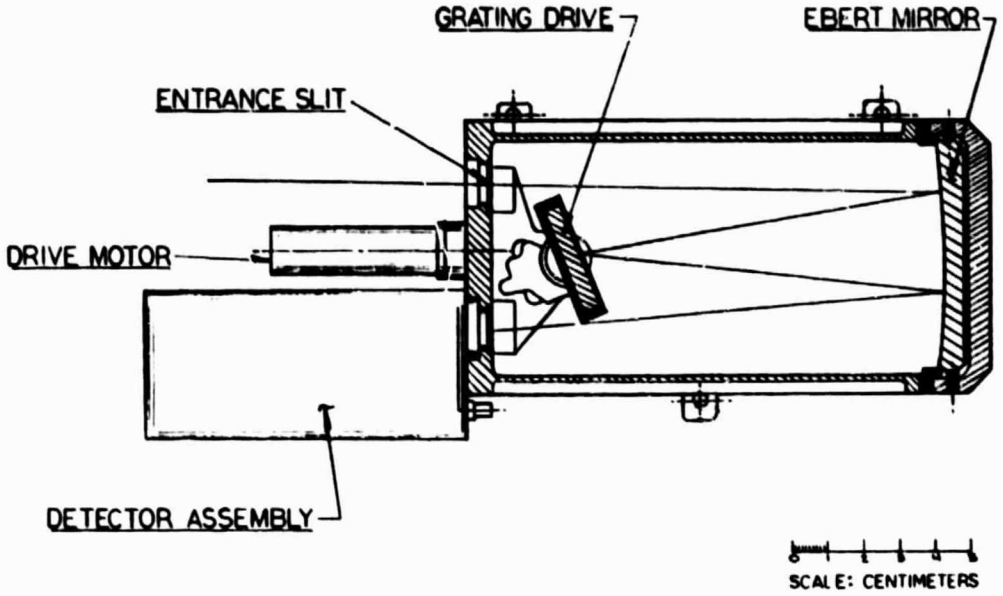

Figure 1. 1/8-meter Ebert-Fastie Spectrometer

For the second flight of the 1/8-meter spectrometers on 15 July 1980, the diffraction grating in the MUV spectrometer was replaced by a new diffraction grating fabricated by Hyperfine, Inc. with a ruling frequency of 2400 grooves mm^{-1}. This allowed measurements of the spectral irradiances over the wavelength range from 1600 to 3184 A with a spectral resolution of 2.1 A. Further details of the calibration of the spectrometers and the results of the 1980 flight are described in the reprint attached to this report (Mount and Rottman, 1981).

Following the termination of this grant, the spectrometers were transferred to Dr. George Mount at the Laboratory for Atmospheric and Space Physics at the University of Colorado under NASA Grant NAG5-212 to continue the program of spectral irradiance measurements during the declining phase of solar cycle 21.

III. 1/4-METER NORMAL-INCIDENCE SPECTROMETER

The requirements for a measurement program of solar spectral irradiances at extreme ultraviolet (EUV) wavelengths in the "windowless" regime below 1250 A dictated by the scientific objectives are, first, an absolute photometric accuracy ranging from ±10% at 1250 A to ±30% at 100 A; and second, a relative photometric accuracy from flight to flight of the order of 1% to 2%. These goals demand a number of instrumental characteristics that are mandatory for accurate spectrophotometry. In particular: 1) windowless operation, 2) low levels of irradiance on the optical components, 3) a hydrocarbon-free environment, 4) a photometrically stable detector system, 5) a low noise detector system, 6) no moving parts within the vacuum chamber, and 7) compatibility with EUV calibration standards such as the National Bureau of Standards (NBS) SURF II Storage Ring calibration facility.

In order to attempt to meet these requirements, a novel, evacuated, EUV spectrometer with a state-of-the-art photoelectric array detector was fabricated under this grant. The spectrometer employs a 1/4-meter radius-of-curvature concave diffraction grating, operating at an angle-of-incidence of 9° in a conventional Rowland circle mounting as shown in the schematic in Fig. 2. The grating ruling frequency is 1028 lines mm^{-1} and the grating is used in the first order to provide a dispersion of 38.7 A mm^{-1}. The entire spectrum from 1250 to 250 A is recorded simultaneously with a (1 x 1024)-pixel Multi-Anode Microchannel Array (MAMA) detector with pixel dimensions 25 microns in width by 6.5 mm in height, as shown in Fig. 3. The coincidence-anode MAMA detector requires a total of only 64 amplifier and discriminator circuits to record the photometric data from the 1024 pixels as described in more detail in the paper by Timothy and Bybee (1981) attached to this report.

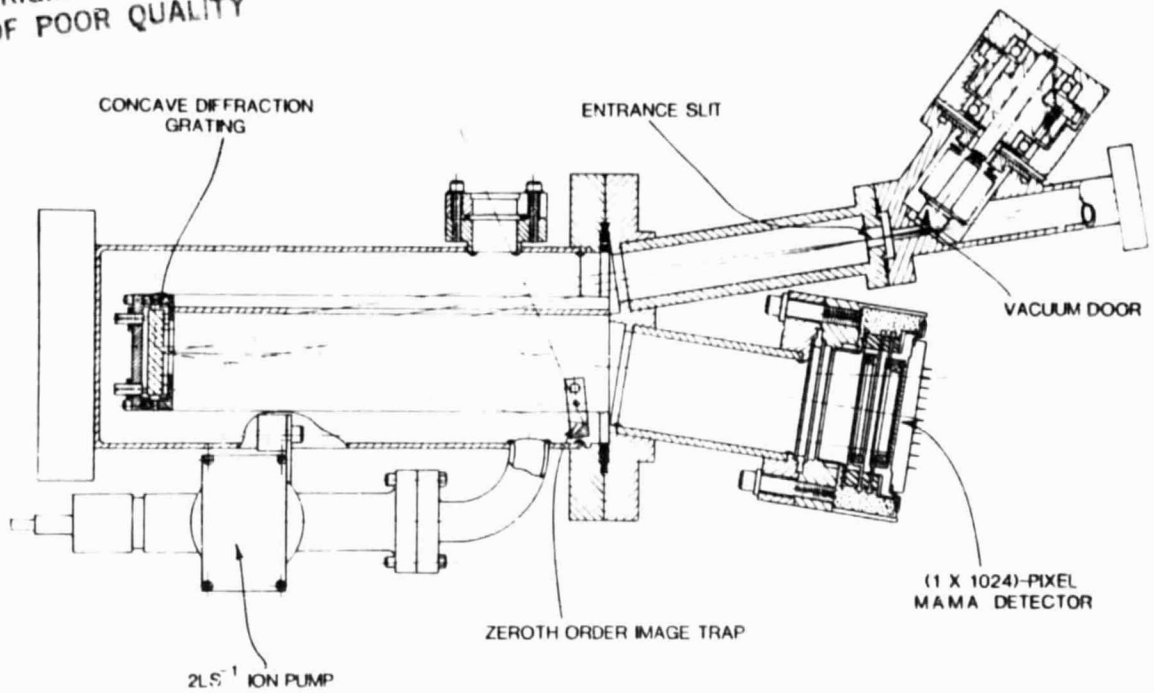

Figure 2. Schematic of 1/4-meter evacuated normal-incidence EUV spectrometer with open-structure (1 x 1024)-pixel MAMA detector.

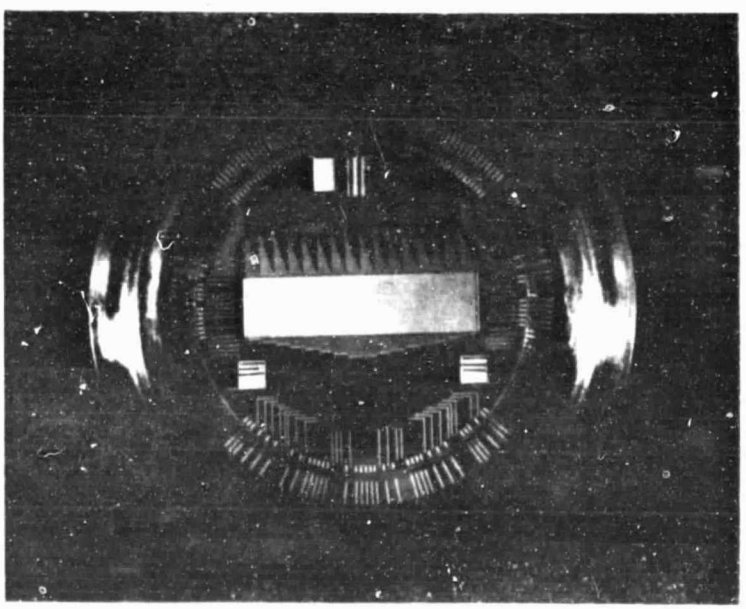

Figure 3. (1 x 1024)-pixel coincidence-anode array with pixel dimensions of 6.5 mm by 25 microns.

The MAMA detector provides a very high photometric stability and very low noise operation (<0.01 counts s^{-1} $pixel^{-1}$) at EUV wavelengths. The spectral resolution is approximately 2 A (2 detector pixels) and the entire spectrum is read out during flight with a temporal resolution of 1.6 s. The spectrometer is evacuated prior to launch, opened for observation during the rocket flight, and re-sealed prior to re-entry. Since there are no moving parts in the spectrometer, a hydrocarbon-free high-vacuum environment is preserved to guarantee the photometric stability of the instrument. The layout of the spectrometer assembly and of the associated electronics modules is shown in Fig. 4.

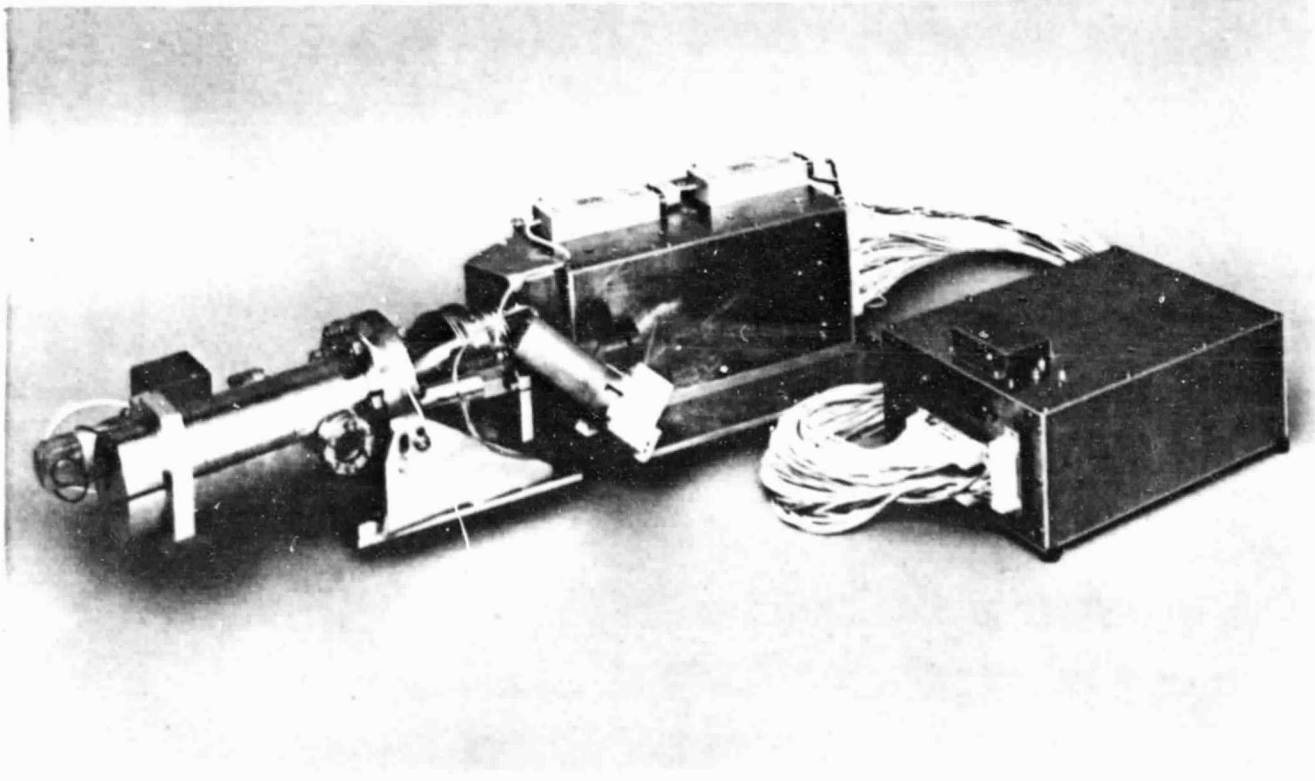

Figure 4. Assembled 1/4-meter normal-incidence EUV spectrometer with electronics assemblies.

It is of particular importance for the photometric measurements to note that the spatial accuracy is printed into the anode array of the MAMA detector system. Photometric errors caused by "rubber cam" effects in scanning spectrometers are accordingly completely eliminated. The detector provides a distortion-free imaging capability which is independent of signal level or of time. As determined from laboratory spectra, such as shown in Fig. 5, the absolute linearity of the detector is of the order of ±2 microns over the 26-mm length of the array.

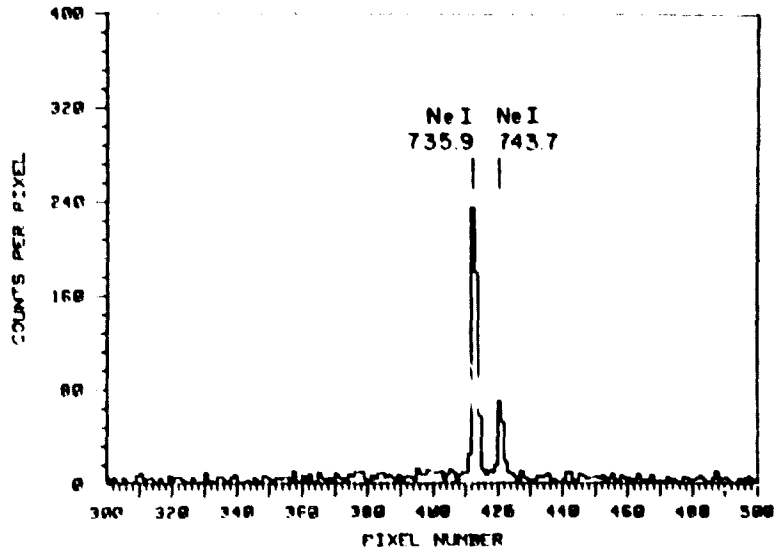

Figure 5. EUV emission lines recorded with 1/4-meter normal-incidence spectrometer.

The pixel-to-pixel crosstalk has been determined to be less than a few percent giving an intensity discrimination between adjacent resolution elements of the order of 10^4:1. The spectrometer and electronics have survived vibration at levels of 20 g over the frequency range from 20 to 2000 Hz without change in the performance characteristics.

The fabrication of the spectrometer was completed in time to undertake an engineering test in an uncalibrated condition on the rocket flight of 15 July 1980. The spectrometer operated correctly for a total of 50 s at the end of the flight and recorded spectra at wavelengths longward of 1200 A in spite of a minor electronics failure. Pressure inside the spectrometer was 2×10^{-7} Torr throughout the launch phase until the vacuum door was opened. At this point, the pressure rose to 8×10^{-5} Torr for the remainder of the flight. Following recovery, the spectrometer was pumped down once more using the internal ion pump to a pressure of 2×10^{-7} Torr. Laboratory tests showed no visible change in the performance characteristics as a result of the flight.

Following the flight, an initial attempt at a calibration on the NBS SURF II Storage Ring was undertaken. In the absence of further funding, only additional engineering work is being undertaken on the 1/4-meter spectrometer as part of the continuing MAMA detector-development program under NASA Grant NSG 7459. However, the spectrometer is in a flight-ready condition and the calibration procedures have now been fully determined. The spectrometer is accordingly ready to undertake a program of spectral irradiance measurements at wavelengths between 1250 and 250 A.

IV. VARIABILITY OF THE SOLAR EXTREME-ULTRAVIOLET SPECTRAL IRRADIANCES

As part of this grant, we have carried out a detailed study of the variability of the solar ultraviolet spectral irradiances over the solar cycle. The full report of this study is contained in a University of Colorado thesis submitted for the MS degree in the Department of Physics (LeFevre, 1982). The primary findings of this study are now being prepared for submission to the literature (Timothy, Zweibel and LeFevre, 1983). The principal result is that, at all wavelengths studied from 1350 to about 300 A, the measured variabilities of the spectral irradiances over solar cycles 20 and 21 significantly exceeded the values predicted on the basis of an increase in the number of

active regions on the solar disk from solar minimum to solar maximum. Because of the large errors in the irradiance measurements, the measured and predicted values agree within the uncertainties for solar cycle 20. However, the predictions are systematically low. For solar cycle 21, with a higher level of solar activity, the disagreements are so large that the measured and predicted values differ by more than the measurement errors. The reasons for this discrepancy are not clear at this time; however, the most probable cause appears to be an increase in the EUV emission from the chromospheric network at solar maximum, probably caused by remnants of old active regions. If verified, this finding is clearly of importance for solar, stellar and atmospheric physics and emphasizes the need for a continuing program of accurate measurements of the solar spectral irradiances at wavelengths below 3000 A. Hopefully, using instruments of the type described in this report and being developed by other groups for both sounding rocket and space shuttle flights, these data will become available during the next solar cycle.

V. REFERENCES

Lefevre, A., Master of Science Thesis, Department of Physics, University of Colorado, 1982.

Mount, G.H., Rottman, G.J. and Timothy, J.G., J. Geophys. Res., 85, 4271, 1980.

Mount, G.H. and Rottman, G.J., J. Geophys. Res., 86, 9193, 1981.

Rottman, G.J., J. Geophys. Res., 86 6697, 1981.

Timothy, J.G. and Bybee, R.L., SPIE Ultraviolet and Vacuum Ultraviolet Systems, 279, 129, 1981.

Timothy, J.G., Zweibel, E. and Lefevre, A., in preparation, 1983.

VI. ATTACHMENTS

"The Solar Spectral Irradiance 1200-2550 A at Solar Maximum" by Mount, G.H., Rottman, G.J. and Timothy, J.G.

"The Solar Spectral Irradiance 1200-3184 A Near Solar Maximum: July 15, 1980" by Mount, G.H. and Rottman, G.J.

"Photon-Counting Array Detectors for Space and Ground-Based Studies at Ultraviolet and Vacuum Ultraviolet (VUV) Wavelengths" by Timothy, J.G. and Bybee, R.L.

JOURNAL OF GEOPHYSICAL RESEARCH, VOL. 86, NO. A11, PAGES 9193-9198, OCTOBER 1, 1981

The Solar Spectral Irradiance 1200–3184 Å Near Solar Maximum: July 15, 1980

GEORGE H. MOUNT AND GARY J. ROTTMAN

Laboratory for Atmospheric and Space Physics, University of Colorado, Boulder, Colorado 80309

Full-disk solar spectral irradiances near solar maximum were obtained in the spectral range 1200–3184 Å at a spectral resolution of approximately 1 Å from rocket observations above White Sands Missile Range, New Mexico, on July 15, 1980. Comparison with measurements made in 1979 and during solar minimum confirms a large increase at solar maximum in the solar irradiance near 1200 Å with no change within our measurement errors near 2000 Å. Irradiances in the range 1900–2100 Å are in excellent agreement with previous measurements, and those in the 2100- to 2500-Å range are lower than the Broadfoot results. We find agreement with previous values 2600–2900 Å and then fall below those values 2900–3184 Å.

INTRODUCTION

Solar radiation at wavelengths shorter than 2980 Å is totally absorbed by the earth's atmosphere and provides the dominant source of energy for atmospheric heating, dissociation, and ionization. An accurate knowledge of the solar spectral irradiance in the ultraviolet is accordingly of fundamental importance for studies of the photochemistry of the upper atmosphere. Unfortunately, because of experimental difficulties, the available data are limited, and there are major uncertainties in many of the measurements.

We have begun a systematic sounding rocket program to study solar ultraviolet irradiance and its variation over the solar cycle. Results from the first flight in this study [*Mount et al.*, 1980], when compared with the solar minimum measurements of *Rottman* [1981], indicate a significant enhancement of irradiance below 1800 Å. Results from the July 15, 1980, rocket flight confirm these conclusions and indicate that the irradiance in the 2100- to 2550-Å spectral region is lower than the *Broadfoot* [1972] results, although not as low as reported in our 1980 paper. Results near 2800 Å are in close agreement with Broadfoot.

FLIGHT INSTRUMENTS

The full-disk solar spectrum from 1160–3184 Å was recorded by two spectrometers that scanned adjacent but overlapping spectral ranges. The spectrometers are designated by the spectral region covered; namely, a far-ultraviolet (FUV) Ebert-Fastie spectrometer with 1/8-m focal length to cover 1160–1850 Å, and a middle-ultraviolet (MUV) Ebert-Fastie spectrometer with 1/8-m focal length to cover 1600–3184 Å. The irradiance payload was not evacuated at launch but was maintained with a dry nitrogen purge for several days prior to launch. The important instrument characteristics are outlined in Table 1.

The irradiance instruments were carried piggyback on a solar rocket with a high-resolution EUV instrument dedicated to the study of coronal holes. The Nike-boosted Black Brant rocket (NASA 27.044 US) reached an altitude of 325 km above White Sands Missile Range, New Mexico, at 1705 UT on July 15, 1980. The solar zenith angle at time of apogee was 23°. All rocket systems performed well and the experiment was completely successful. Just prior to launch, the spectrometers were individually aligned with the Solar-Pointing Aerobee Rocket Control System (SPARCS) to ±1 arc minute. Mechanical alignment of the instruments was checked immediately after recovery and was found to be unchanged by the flight and recovery. The MUV spectrometer calibration was checked 63 days after the flight and was found to be unchanged from pre-flight values. The FUV spectrometer was damaged on impact. Impact during the recovery phase caused an internal misalignment of the FUV spectrometer optics and precluded a post-flight calibration.

INSTRUMENT CALIBRATION

The absolute efficiencies of the flight spectrometers were measured at the Johns Hopkins University as described in detail by *Mount et al.* [1980]. Briefly, the Johns Hopkins calibration test equipment (CTE) compares the monochromatic response of calibrated reference photomultiplier tubes with the response of the instrument under test. The reference photomultiplier tubes are calibrated before and after instrument tests against National Bureau of Standards standard photodiodes 1[illegible]95 and 17183 [*Canfield et al.*, 1973]. The FUV calibration was made with the same error budget as for the 1979 flight. The MUV spectrometer, however, was calibrated with a larger error budget as shown in Table 2.

The source of the larger over-all error for the MUV spectrometer was an instability in the Johns Hopkins CTE reference *f* photomultiplier tube. This instability has been noted previously [*Brune et al.*, 1979] and resulted in a larger transfer error between the NBS photodiode and the reference photomultiplier tube.

The FUV spectrometer experienced no calibration difficulties during the pre-flight calibration. No direct post-flight calibration was possible due to damage on impact that misaligned the optics. The MUV spectrometer was recalibrated at Johns Hopkins after the flight with agreement to ±8%. The pre-flight calibration was used in the data reduction. The 1979 calibrations indicate no change before and after the flight on either of the two spectrometers flown to within ±5%.

In addition to the calibration at Johns Hopkins, the MUV spectrometer was calibrated with an NBS standard tungsten lamp in our laboratory. The overlap region of the two calibrations was approximately 2600–3000 Å and the spectrometer efficiencies derived from these two independent methods agree within 10% near 2700 Å and 20% near 3000 Å. Figure 1 shows the calibration of the MUV instrument with associated

Paper number 1A0764.
0148-0227/81/001A-0764$01.00

TABLE 1. Instrument Characteristics

Parameter	FUV	MUV
Spectrometer type	Ebert-Fastie	Ebert-Fastie
Focal length, mm	125	125
Spectral range, Å	1160–1850	1600–3184
Grating		
Ruled area, mm	26 × 26	26 × 26
Ruling frequency, g/mm	3600	2400
Coating	Al-MgF_2	Al-MgF_2
Manufacturer	Bausch and Lomb	Hyperfine, Inc.
Scan period, S	12	12
Detector	EMR 510G MgF_2 window	EMR 510F MgF_2 window
Field of view	11°.5	11°.5
Slits		
Entrance area, mm^2	0.048 × 0.752	0.048 × 1.00
Exit area, mm^2	0.056 × 3.00	0.071 × 3.00
Filter (interference)	None	1800 Å Broadband
RMS grating drive jitter	±0.3 Å	±0.3 Å
Spectral Resolution	1.15 Å @ Ly α	2.10 Å @ 2500 Å
Step size	0.28 Å @ Lyα	0.45 Å @ 2500 Å

TABLE 2. Error Budgets

Parameter	FUV	MUV
NBS standard diode	±6%	±6–10% (1600–3000 Å)
CTE transfer to PMT	±8%	±12%
Slit width		
Entrance	±4%	±4%
Exit	±4%	±4%
Efficiency variation across field of view	±3%	±3%
Geometrical errors estimate	±5%	±5%
Difference: JHU calibration—LASP NBS tungsten lamp calibration	...	10% (at 2700 Å)
Interference filter	...	3%
Instrument scattered light	<0.3% of peak signal	<0.3% of peak signal
Quadrature sum	13%	16–21%

absolute error bars (see Table 2). The adopted curve falls between the Johns Hopkins and the tungsten lamp calibrations.

A major source of calibration error occurs in the measurement of the small slit widths (approximately 50 μ) used on the spectrometers. Errors were ±4% and the slits were measured on three different engines and using diffracted red laser light.

The instruments were rotated ±5° about the incident beam at Johns Hopkins to provide a map of the grating and Ebert mirror. Non-uniformities were less than ±3%, insuring that a small misalignment in solar pointing does not introduce a calibration uncertainty.

The total error budget was ±13% for the FUV spectrometer and ±18% for the MUV spectrometer (see Table 2).

Results and Discussion

The data were analyzed as described in *Mount et al.* [1980]. Figure 2 (FUV) and Figures 3–6 (MUV) show the results (including all line fluxes) averaged into 10-Å bins and compared with other measurements. Absolute error bars are indicated. Table 3 lists the data corrected to 1 AU, averaged into 10-Å bins, and including all line fluxes. The daily Zurich sunspot number R_z was 207 for the 1979 flight and 165 for the 1980 flight. Of the 35 complete scans obtained by each spectrometer during the flight, only 10 scans were used, all recorded above 275 km. Statistical uncertainty was less than ±2% for each wavelength bin.

Comparison of the 1979 and 1980 flight results (Figure 2) indicates essentially no change in the solar irradiance 1200–1900 Å within our measurement accuracy. The relative irradiance values of the 1979 and 1980 flights are of particular significance since the same FUV spectrometer was flown. The instrument was not dismantled or disturbed in the intervening year and was stored in a clean, dessicated environment. The calibration values obtained for the 1980 flight from the same calibration facility were within 10% of the 1979 values, with the largest difference below 1350 Å. This difference is almost certainly calibration error and not a change in actual instrument sensitivity. Thus, comparison of the 1979 and 1980 results with the solar minimum results of *Rottman* [1981] (also taken with the same instrument) confirms our earlier conclusion [*Mount et al.*, 1980] that there is significant variability in the solar spectral irradiance from solar minimum to solar maximum at wavelengths short of 1800 Å and that the change varies from less than the measurement error at 2000 Å to a factor of 2.5 near 1200 Å. The effective brightness temperature of the atmospheric temperature minimum calculated at 1600 Å is 4654°K.

The important comparison to be made in Figure 2 is between Rottman's solar minimum results and our solar maximum results, since the same instrument was used to take both data sets. The solar minimum data and its comparison with (e.g.) *Heroux and Swirbalus* [1976] are discussed in detail by *Rottman* [1981]. Briefly, it seems clear that most of the difference between the Rottman results and those of Heroux and

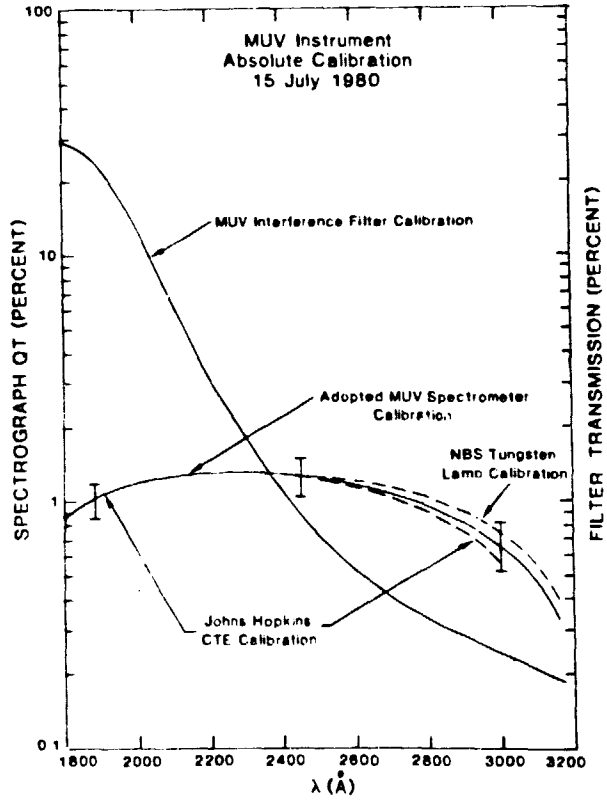

Fig. 1. The absolute calibrations of the MUV interference filter and the MUV spectrograph. Note the difference in calibration above 2800 Å between the Johns Hopkins CTE (based on NBS standard photodiodes) and an NBS tungsten lamp source.

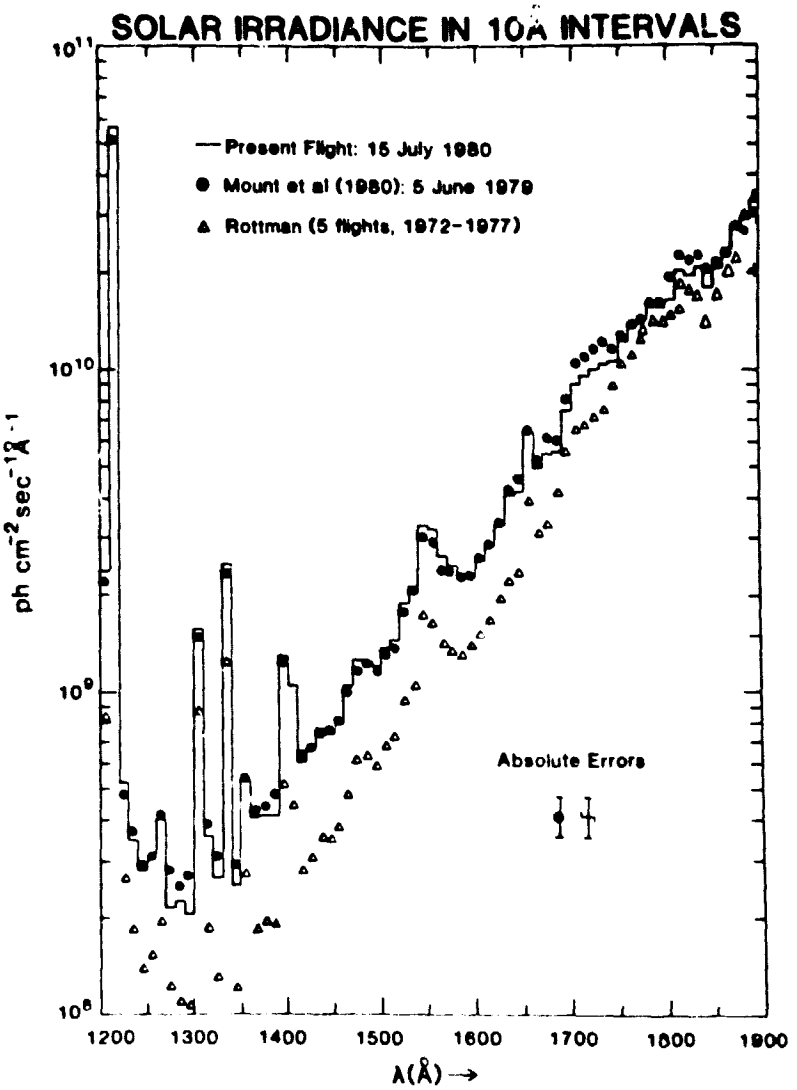

Fig. 2. Solar irradiance in the spectral range 1200–1900 Å averaged into 10 Å bins including line fluxes and compared with our 1979 flight results and those of *Rottman* [1981] at solar minimum. The data have been corrected to 1 AU. Present results are listed in Table 3.

Swirbalus is caused by a calibration problem and not an intrinsic change in solar irradiance during solar minimum.

The MUV results are shown in Figures 3–6. Below 2100 Å we find agreement with the many measurements made in that spectral region [*Bruecl ner et al.*, 1976; *Samain and Simon*, 1976; *Simon*, 1975]. The 1980 measuremcnts are higher than the average by about 14%, and the 1979 results are lower by about 14%.

In the spectral region 2100–2550 Å, we find a large difference (40%) between our 1979 and 1980 results with agreement closer to, but still 20% below, the *Broadfoot* [1972] values. Figure 6 shows the comparison with a 20 Å running average. Since the MUV instrument was rebuilt for the 1980 flight to extend the spectral coverage from 2550 Å to 3184 Å, a true relative comparison of the results is not possible. The same phototube and electronics were used on both flights; however, in addition to replacement of the grating, an 1800-Å broadband interference filter was included to reduce the dynamic range requirement on the detector. The calibration of the filter is shown in Figure 1. Since its calibration is a relative measurement, errors are less than a few percent. The measurements made in our laboratory agreed to within 3% of the manufacturer's (Acton Research Corporation) results.

We have continued laboratory testing of the MUV instrument since the 1980 flight in order to locate the source of the discrepancy between the two data sets. We have found a temperature effect in the detector electronics that produces a decreasing count rate with increasing temperature for constant light input. At 60°C this effect is approximately 15%. Summing total counts per scan on the 1979 flight indicates a 14% sag in count rate later in that flight. Only a 3% effect was observed on the 1980 flight. Since the temperatures of the instruments were not monitored during the flight, we do not know their exact temperatures. However, based on detailed temperature measurements of the solar cor .al hole instrument, it is not unreasonable to expect the te nperature on the MUV instrument to have reached 60°C. Temperature tests made immediately after the 1979 flight did not go to 60°C. Thus we may conclude that the data from the MUV instrument on the 1979 flight could be raised approximately 15%. This reduces the difference between the two sets of flight data to approximately 25% and raises the MUV data to the

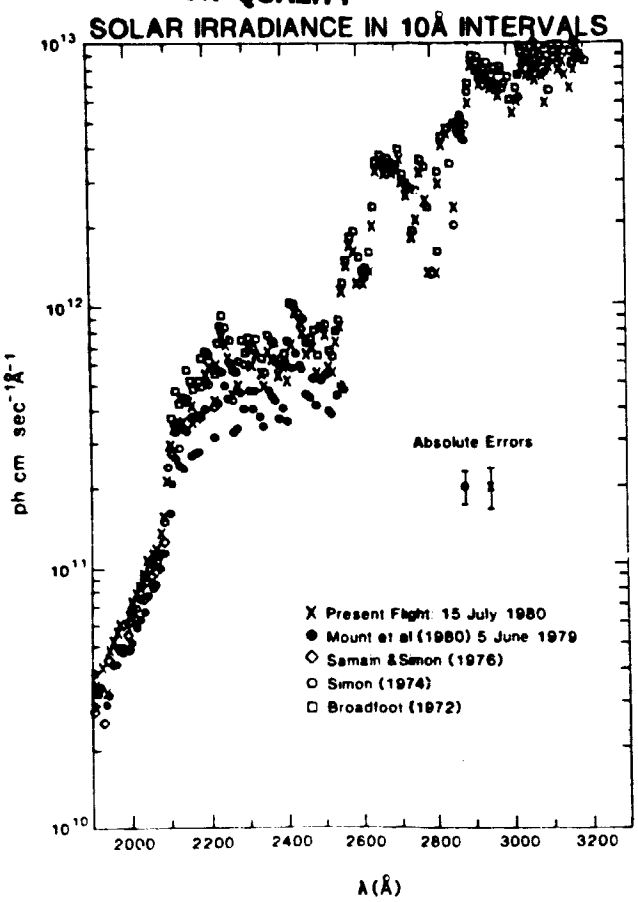

Fig. 3. Solar irradiance in the spectral range 1900–3200 Å averaged into 10-Å bins and compared with previous results. The data have been corrected to 1 AU. Present results are listed in Table 3.

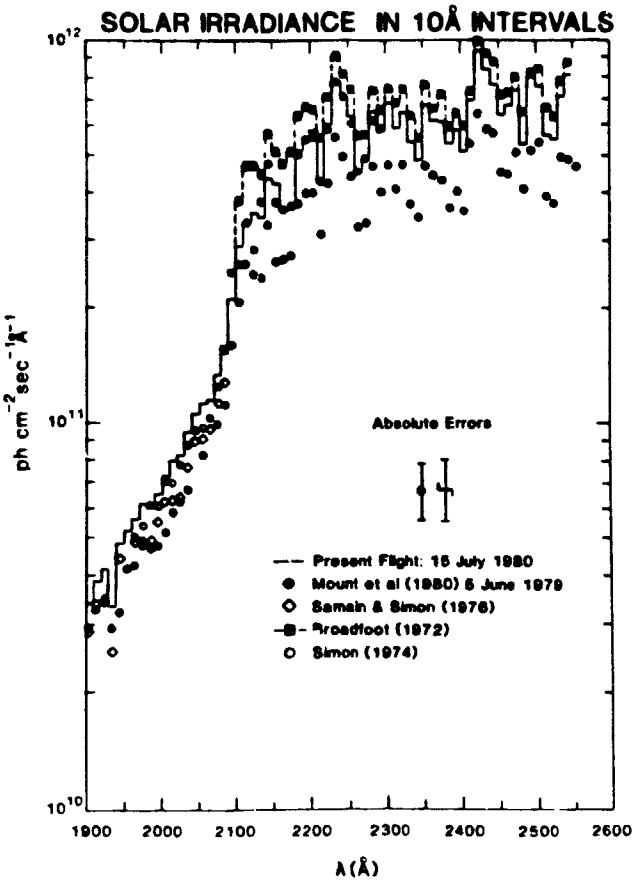

Fig. 4. Same as Figure 3 except 1900–2600 Å.

average of the many 1900- to 2100-Å measurements. The residual difference is attributed to calibration and slit measurement errors, assuming a variation in the solar irradiance much smaller than the ±18% error bars. The 1979 MUV data below 1900 Å were merged with the FUV data at 1800 Å. Thus we recommend no change in the 1979 results below 1800 Å, but would increase those results 15% above 1900 Å.

From 2550 to 2900 Å we find close agreement of our results with *Broadfoot* [1972]. Above 2900 Å we once again fall below the Broadfoot results. Our calibration above 2800 Å is not as reliable as below that wavelength (see Figure 1) due to disagreement between the CTE and tungsten lamp calibrations. We have placed our calibration curve between the two measured calibration curves above 2600 Å. The reader is referred to a recent review by *Kohl et al.* [1980] for a comparison of the Broadfoot results with other investigators.

It is very important to note that all the data taken on both flights were full solar disc measurements. Thus, no assumptions about limb darkening have been introduced into the analysis as would be required on data obtained with a solar instrument with a restricted field of view.

In addition to measuring the continuum irradiance, we measured the absolute intensities of several strong emission lines of atomic species. Results are given in Table 4 along with ratios to solar minimum. In all cases the appropriate continuum background was subtracted before the integral of the line profile was calculated.

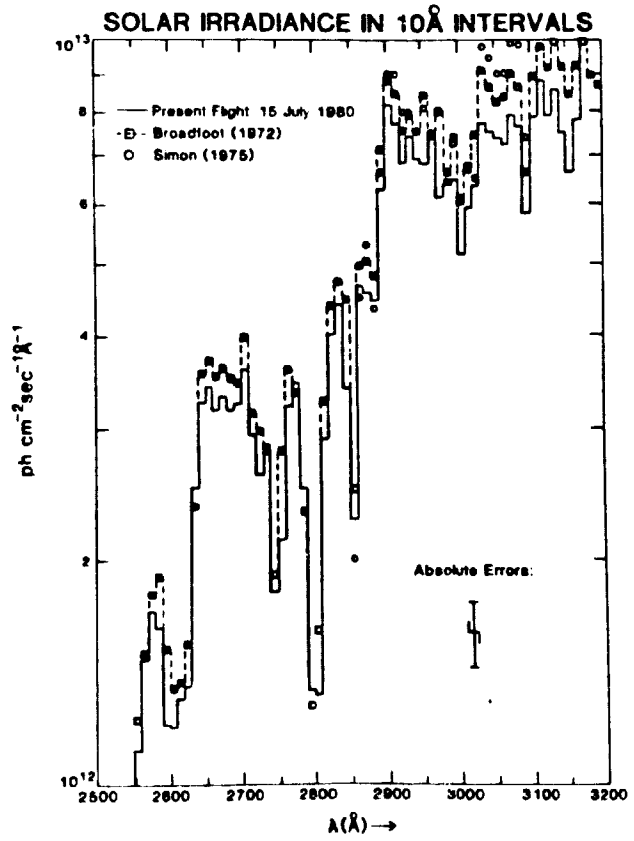

Fig. 5. Same as Figure 4 except 2600–3184 Å.

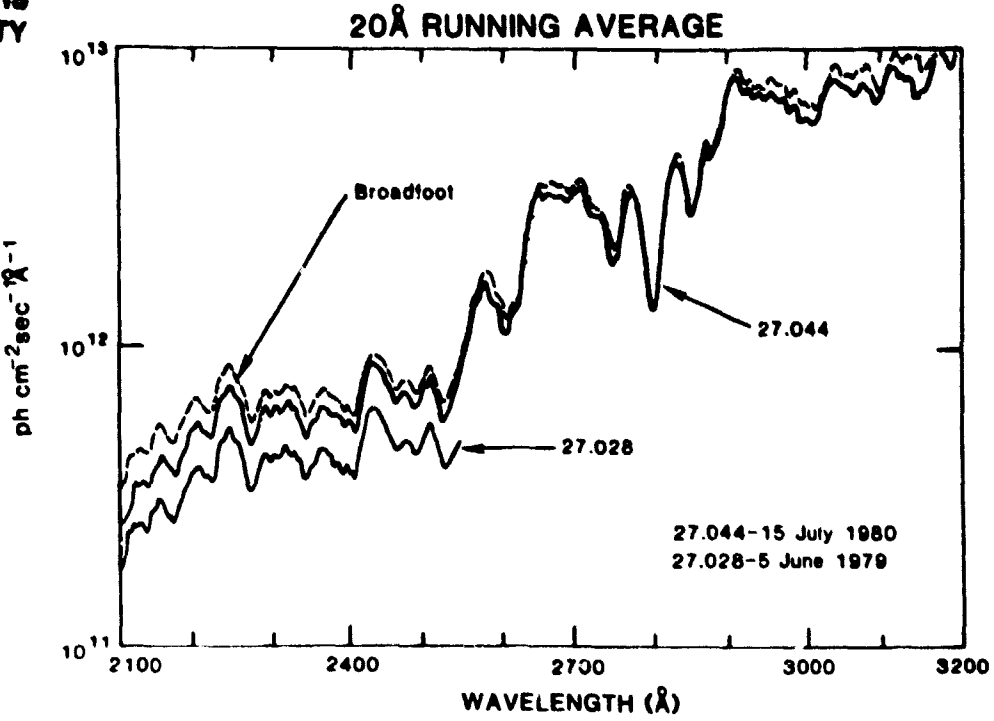

Fig. 6. A 20 Å running sum comparison of our 1979 and 1980 flight results and those of *Broadfoot* [1972].

CONCLUSIONS

We confirm our conclusion from the June 5, 1979 flight that there is significant variability in the solar spectral irradiance from solar minimum to solar maximum at wavelengths short of 1800 Å with the change varying from less than the measurement error near 2000 Å to a factor of 2.5 near 1200 Å. We find good agreement among recent investigations in the 1900- to 2100 Å region. We conclude that the irradiance values of *Broadfoot* [1972] from 2100-2500 Å lie within our mutual error bars although both 1979 and 1980 results fall somewhat below Broadfoot's results, and we find reasonable agreement with the measurements of both *Broadfoot* [1972] and *Simon* [1980] above 2600 Å.

We are presently testing a new ultraviolet calibration facility that will improve our understanding of the flight instrument, especially at longer wavelengths.

Acknowledgments. We wish to express our appreciation to both the NASA and Lockheed teams at White Sands Missle Range responsible for the successful flight. We thank W. G. Fastie for use of the CTF calibration system at Johns Hopkins University. This work was supported by NASA Office of Applications grant NSG 7559 and flew on a rocket supported by NASA Solar Physics Office grant NSG 5178. A portion of our laboratory calibration of these rocket instruments has been supported by NOAA research grant NA80RAC00112.

The Editor thanks H. E. Hinteregger for his assistance in evaluating this paper.

TABLE 3. Solar Irradiance in Units of 10^{10} ph cm^{-2} s^{-1} Å^{-1} Averaged in 10 Å Intervals at 1 AU for Rocket Flight 27.044, July 15, 1980

Wavelength, Å	Interval, Å									
	00-10	10-20	20-30	30-40	40-50	50-60	60-70	70-80	80-90	90-100
1200	0.236	5.64	0.052	0.035	0.028	0.031	0.041	0.021	0.022	0.021
1300	0.154	0.036	0.026	0.251	0.025	0.053	0.041	0.041	0.041	0.128
1400	0.105	0.060	0.066	0.076	0.074	0.079	0.104	0.125	0.122	0.119
1500	0.136	0.143	0.187	0.212	0.327	0.315	0.258	0.244	0.223	0.223
1600	0.253	0.280	0.326	0.404	0.411	0.634	0.491	0.542	0.554	0.745
1700	0.900	0.953	0.999	1.02	1.05	1.22	1.39	1.42	1.54	1.60
1800	1.63	2.01	1.94	2.05	1.80	2.05	2.37	2.77	2.91	3.31
1900	3.41	3.86	4.15	3.31	4.85	5.25	5.62	6.13	6.07	6.54
2000	7.23	7.93	8.26	9.44	10.5	11.2	11.5	13.4	15.2	21.2
2100	29.1	33.3	35.6	34.6	43.4	42.2	36.1	36.6	51.7	54.4
2200	58.1	42.9	59.9	77.9	70.7	62.9	45.1	49.1	65.3	57.5
2300	68.8	59.4	65.4	54.2	48.7	67.8	61.8	61.5	53.6	58.5
2400	51.0	70.0	93.9	84.9	77.3	64.6	67.9	75.0	54.3	81.8
2500	76.6	56.9	55.5	71.6	81.7	112	146	169	161	120
2600	119	129	135	251	324	342	317	330	318	324
2700	357	293	260	286	182	212	321	346	249	133
2800	131	289	401	440	339	226	469	457	444	639
2900	816	771	683	739	692	681	736	611	640	644
3000	508	593	635	777	749	735	719	790	764	585
3100	785	879	789	853	746	665	778	1050		

TABLE 4. Absolute Line Fluxes (ph cm^{-2} s^{-1})

Species	Wavelength, Å	June 5, 1979	July 15, 1980	Ratio [Solar Maximum/Solar Minimum]* June 5, 1979†	Ratio [Solar Maximum/Solar Minimum]* July 15, 1980
Si III	1206.53	1.7E10	1.50E10	3.1	2.7
H Ly	1215.68	4.36E11	5.01E11	1.4	1.6
N V	1238.82	7.1E8	8.7E8	...	...
	1242.80	5.3E8	5.6E8	...	...
Si II	1260.42	4.9E8	6.9E8	...	...
Si II	1264.74	9.2E8	1.5E9	...	...
O I	1302.17	4.7E9	3.4E9	1.9	1.4
O I	1304.86	9.3E9	9.8E9	1.7	1.8
O I	1306.03				
C II	1334.53	2.2E10	2.6E10	2.2	2.7
	1335.66				
O I	1355.60	9.6E8	1.0E9	1.5	1.6
Si IV	1393.76	7.4E9	7.3E9	2.2	2.2
Si IV	1402.77	3.3E9	3.4E9		
Si II	1526.71	4.20E9	2.3E9	...	...
C IV	1548.20	1.6E10	1.5E10	2.2	2.1
C IV	1550.77	6.9E9	7.4E9	1.7	1.9
C I	1561 (multiplet)	6.8E9	1.0E10	1.4	2.1
He II	1640.33 (Fe II blend?)	9.4E9	5.1E9	...	...
C I	1657 (multiplet)	2.7E10	2.1E10	1.8	1.4
Si II	1808.01	1.3E10	1.3E10	...	...
Si II	1816.93, 1817.45	2.6E10	4.5E10	0.8	1.3

* *Rottman* [1981].
† Revised. See *Rottman* [1981].

REFERENCES

Broadfoot, L., The solar spectrum 2100–3200 Å *Astrophys. J., 173*, 681, 1972.

Brueckner, G., J. Bartoe, O. Kjeldseth-Moe, and M. Van Hoosier, Absolute solar ultraviolet intensities and their variations with solar activity, I, The wavelength region 1750–2100 Å, *Astrophys. J., 209*, 935, 1976.

Brune, W., G. Mount, and P. Feldman, Vacuum ultraviolet spectrophotometry and effective temperatures of hot stars, *Astrophys. J., 227*, 884, 1979.

Canfield, L., R. Johnston, and R. Madden, NBS detector standards for the ultraviolet, *Appl. Opt., 12*, 1611, 1973.

Heroux, L., and R. A. Swirbalus, Full-disk fluxes between 1230 and 1940 Å, *J. Geophys. Res., 81*, 436, 1976.

Kohl, J., W. Parkinson, and C. Zapata, Solar spectral radiance and irradiance at 225.2–319.6 nm, *Astrophys. J. Suppl., 44*, 295, 1980.

Mount, G., G. Rottman, and J. Timothy, The solar spectral irradiance 1200–2550 Å at solar maximum, *J. Geophys. Res., 85*, 4271, 1980.

Rottman, G., Rocket measurements of the solar spectral irradiance during solar minimum, 1972 to 1977, *J. Geophys. Res., 86*, in press, 1981.

Samain, D. and P. C. Simon, Solar flux determination in the spectral range 150–210 nm, *Solar Phys., 49*, 33, 1976.

Simon, P. C., Nouvelles mesures de l'ultraviolet solaire dans la stratosphere, *Bull. Cl. Sci Acad R. Belg., 61*, 399, 1975.

Simon, P. C., Observation of the solar ultraviolet radiation, *Aeronomica Acta, 211*, 1, 1980.

(Received March 18, 1981;
revised May 4, 1981;
accepted May 5, 1981.)

JOURNAL OF GEOPHYSICAL RESEARCH, VOL. 85, NO. A8, PAGES 4271–4274, AUGUST 1, 1980

The Solar Spectral Irradiance 1200–2550 Å at Solar Maximum

GEORGE H. MOUNT, GARY J. ROTTMAN, AND J. GETHYN TIMOTHY

Laboratory for Atmospheric and Space Physics, University of Colorado, Boulder, Colorado 80309

Full-disk solar spectral irradiances at solar maximum were obtained in the spectral range 1200–2550 Å at a spectral resolution of approximately 1 Å from rocket observations above White Sands, New Mexico, on June 5, 1979. Comparison with measurements made near solar minimum indicates approximately a factor of 2.5 increase in the irradiance at 1200 Å, a 20% increase near 1800 Å, and no increase within our measurement errors (±15%) above 2100 Å. Irradiances in the range 1800–2100 Å are in excellent agreement with previous measurements, but those in the 2100- to 2550-Å range are significantly lower. The intensities of strong emission lines at wavelengths below 1850 Å are also reported.

INTRODUCTION

Solar radiation at wavelengths shorter than 2980 Å is totally absorbed by the earth's atmosphere and provides the dominant source of energy for atmospheric heating, dissociation, and ionization. An accurate knowledge of the solar spectral irradiances in the ultraviolet is accordingly of fundamental importance for studies of the photochemistry of the upper atmosphere. Unfortunately, because of experimental difficulties, the available data are extremely limited, and there are major uncertainties in many of the measurements. In particular, the magnitude of the variability of the spectral irradiances over the solar cycle has not been determined.

As the first stage of a systematic study of this problem, two spectrometers were flown to measure the solar irradiances in the wavelength range from 1200 to 2550 Å near solar maximum. It was found that solar maximum irradiances are significantly larger than the solar minimum irradiances in the spectral region below 1800 Å. The measured irradiances above 2100 Å were lower than previously accepted values.

FLIGHT INSTRUMENTS

The full-disk solar spectrum from 1160 to 2550 Å was recorded by two spectrometers which scanned adjacent but overlapping spectral ranges. The spectrometers are designated by the spectral region covered, namely, a far-ultraviolet (FUV) spectrometer, a ¼-m focal length Ebert-Fastie spectrometer for the range 1160–1850 Å, and a middle-ultraviolet (MUV) spectrometer, a ¼-m focal length Ebert-Fastie spectrometer for the range 1600–2550 Å. The important instrument characteristics are outlined in Table 1.

The instruments were launched on a Nike-boosted Black Brant rocket (NASA 27.028 US) to an altitude of 325 km above White Sands Missile Range, New Mexico, at 1715 UT on June 5, 1979. The solar zenith angle at the time of apogee was about 20°. The rocket performed perfectly, and the excellent condition of the recovered payload permitted postflight instrument calibrations. Just prior to launch, the spectrometers were individually aligned with the solar pointing Aerobee Rocket control system (SPARCS) to ±1 arc min. Instrument optical alignments were checked immediately after recovery and were found to be unchanged by the flight. Spectrometer calibrations were checked 13 days after the flight and were found to be unchanged from preflight values.

INSTRUMENT CALIBRATION

The absolute efficiencies of the spectrometers were measured at the Johns Hopkins University. The calibration test equipment (CTE), described by *Fastie and Kerr* [1975], has an *f*/80 monochromatic beam which can be directed to either the instrument under test or to a reference detector. All radiation measured by the calibrated reference detector passes through the test instrument entrance slit which is at the beam focus. Two light sources, a low pressure H_2 lamp [*Fastie and Kerr*, 1975] and a Pt-Ne hollow cathode lamp [*Mount et al.*, 1977], provide line spectra dispersed at 2-Å resolution by the CTE premonochromator. The reference detectors, EMR G and Hamamatsu F photomultiplier tubes for spectral ranges 1160–1700 Å and 1700–3200 Å, respectively, were calibrated against National Bureau of Standards (NBS) standard photodiodes 17195 and 17183 [*Canfield et al.*, 1973]. The NBS-quote uncertainty for the photodiode calibrations of July 1978 is ±6% from 1200 to 1700 Å and then gradually increases to ±10% at 3100 Å. Error in the calibration transfer from the photodiodes to the FUV and MUV spectrometers is ±6% and ±8%, respectively. The higher uncertainty at longer wavelengths is due to technical difficulties stemming from instabilities in the CTE reference detector. These errors were determined by repeated calibrations of several rocket instruments used at Johns Hopkins and represent a maximum and not a mean uncertainty. Independently, *Guenther and Williams* [1979] indicate that the NBS Synchrotron Users Radiation Facility (SURF) calibration and the Johns Hopkins calibrations agree to within 5% in the 1450- to 1800-Å region. Preflight and postflight calibrations for the instruments agreed to within 5% at all wavelengths measured. An independent postflight calibration above 2400 Å was performed on the MUV spectrometer with an NBS-calibrated standard tungsten-strip filament lamp (EUV 119). The measured spectrometer efficiencies derived are within 5% of the Johns Hopkins CTE calibration.

As an in-flight calibration cross-check, a 250-Å overlap region was scanned by the two spectrometers. Although only 150 Å of this was useful because of the low signal level between 1600 and 1700 Å in the MUV instrument, the 150-Å overlap region agreed to within 5% from 1700 to 1750 Å and to within 10% from 1750 to 1850 Å.

A major source of calibration error occurs in the measurement of the small slit widths (approximately 50 μ) used in the spectrometers. Slit widths were measured on two independent traveling microscopes by three different people, and also by single-slit diffraction using the neon laser red line. The measurement accuracy was ±8%.

The responses of both spectrometers were carefully mapped over the full collection areas, since during flight the solar disk was scanned over ±17 arc min by the SPARCS pointing system (an extreme ultraviolet instrument with a small field-of-view was also on board). Efficiency variations were less than

Paper number 80A0416
0148-0227/80/080A-0416$01.00

TABLE 1. Instrument Characteristics

Parameter	FUV	MUV
Spectrometer type	Ebert-Fastie	Ebert-Fastie
Focal length, mm	125	125
Spectral range, Å	1160–1850	1605–2550
Spectral resolution, Å	1.2	1.4
Grating		
Ruled area, mm	26 × 26	26 × 26
Ruling frequency, g/mm	3600	3600
Coating	Al with MgF_2	Al with MgF_2
Scan period, s	12	12
Detector	EMR 510 G*	EMR 510 F*
Field of view	11.5°	11.5°
Slits		
Entrance area, mm	0.051 × 0.508	0.052 × 0.108
Exit area, mm	0.064 × 3.00	0.078 × 3.00

*MgF_2 window.

±3% across the fields of view, and no correlation could be found of the measured irradiance with the disk position during the flight.

The spectrometers were illuminated in the laboratory by light intensities similar to those observed during the flight to check for photomultiplier fatiguing. No fatiguing was measured. In addition, the temperature response of the flight electronics was tested, and no sensitivity to temperature was observed for the expected flight temperatures.

Instrument-scattered light was measured outside the region of instrument sensitivity to be less than 0.3% of the peak measured signal. When a reasonable uncertainty of 5% for geometrical factors in the overall instrument efficiencies is included, the absolute calibration uncertainty for the FUV spectrometer is ±12% and for the MUV spectrometer is ±15%.

Data Analysis

The photomultiplier signals were pulse counted and telemetered to ground by a PCM (pulse count modulation)/FM system. The output pulses from each spectrometer were summed into 3.2-ms sampling bins, which corresponds to a bin resolution of approximately 0.3 Å. The data were converted to units of photons $cm^{-2}\ s^{-1}\ Å^{-1}$ by application of the efficiency and wavelength calibration data. The absolute wavelength calibration is accurate to better than ±3 Å and was repeatable during the flight to ±1 bin (±0.3 Å).

Thirty-three complete solar scans were obtained by each spectrometer. Of these, the first 10 scans were subject to instrument outgassing, as indicated by summing the total counts observed during the scan. Only 10 scans of the FUV instrument and 7 scans of the MUV instrument recorded at altitudes above 275 km were used as the final data set. The counts from these scans were averaged. Electronic noise was completely negligible, and an electronic dead time correction was applied to all the data using the expression

$$C_{real} = \frac{C_{obs}}{(1 - \tau C_{obs})}$$

where τ is the electronic dead time; τ was carefully measured as 225 ± 10 ns. The dead time correction was negligible except at Ly α 1216 Å (22% correction) and in the region above 2100 Å (7–12% correction).

Results and Discussion

Figures 1 (FUV) and 2 (MUV) show the data (including line fluxes) averaged into 10-Å bins and compared with previous measurements. Absolute error bars are indicated. Table 2 lists the data corrected to 1 AU, averaged in 10-Å bins, and including all lines fluxes. Comparison of the solar maximum with the solar minimum irradiances in Figure 1 shows a large (approximately a factor of 2.5) increase in the irradiance at wavelengths near 1200 Å with a monotonically decreasing variability at longer wavelengths. No variability outside of the measurement accuracy is observed at wavelengths longer than about 2000 Å.

G. Rottman's unpublished data (1980) in the spectral region 1200–1800 Å are used for comparison, since these data were recorded with the same instruments which were calibrated on the same facility. This eliminates the major source of error in comparing data from different sources. Rottman's data are the average of five rocket flights made between 1972 and 1976 (solar minimum) with an average approximately 30% higher than the average of the results of the first two flights [*Rottman*, 1974], which are reported in the review of *Heath and Thekaekara* [1977]. Total variance of the five flights is approximately 20% and is discussed in detail by G. Rottman (unpublished data, 1980). The five-flight average was used for comparison here in order to minimize problems associated with the 'snapshot' nature of rocket flights. *Heath and Thekaekara* [1977] compare Rottman's 1974 results with the data of other authors.

The increase in the irradiances from solar minimum to solar maximum has been independently confirmed by the Atmosphere Explorer satellite data [*Hinteregger*, 1979], which indicate an approximate 2.5 increase from 1200 to 1300 Å and a 20% increase near 1800 Å from July 1976 to January 1979 in 10-Å-averaged intervals. Although the sun was quite active at the time of the flight on June 5 ($R_Z = 207$, $F_{10.7} = 230.2$), a factor of 2.5 increase in the irradiance cannot be explained simply on the basis of an increase in the number of active regions on the solar disk, as will be discussed by G. Rottman (unpublished data, 1980). *Heath* [1973] has shown from Nimbus 3

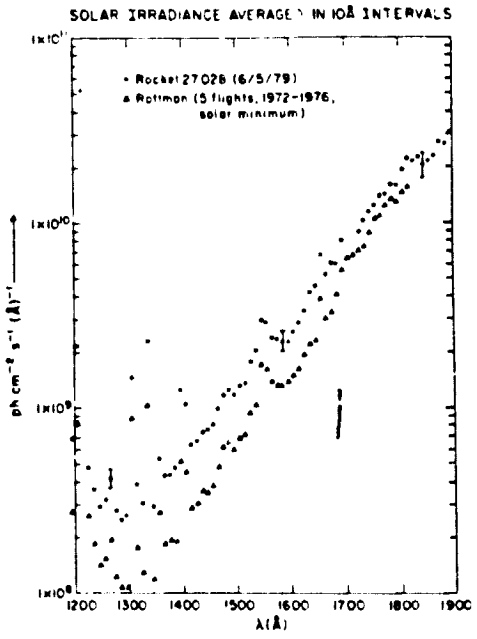

Fig. 1. Solar irradiances in the spectral range 1200–1900 Å averaged into 10-Å bins including line fluxes and compared with G. Rottman's (unpublished data, 1980) five-flight solar minimum results. The data have been corrected to 1 AU. Present results (solid circles) are listed in Table 2.

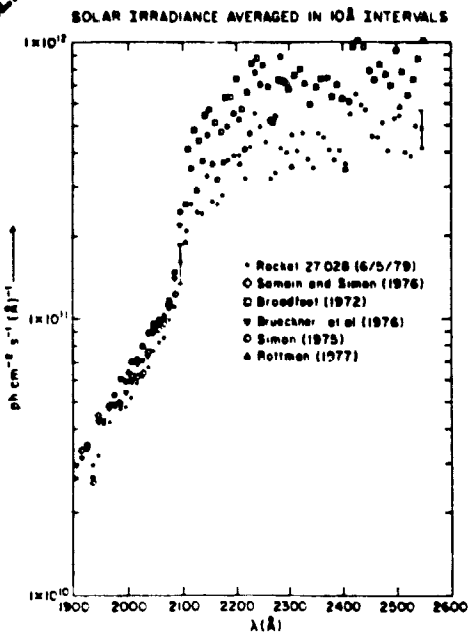

Fig. 2. Solar irradiances in the spectral range 1900–2550 Å averaged into 10-Å bins and compared with previous results. The data have been corrected to 1 AU. The large variation in irradiance above 2100 Å is caused by Fraunhofer structure. Present results (solid circles) are listed in Table 2.

measurements that the maximum expected variation over the 27-day solar rotation period caused by active regions is about 30% from 1200 to 1300 Å and that it decreases to longer wavelengths.

Figure 2 shows the MUV results to be in close agreement with the many measurements made below 2100 Å (*Broadfoot* [1972]; *Brueckner et al.* [1976]; *Samain and Simon* [1976]; *Simon* [1975]; see also *Simon* [1978]). Above 2100 Å, however, the irradiance data are significantly lower than the data of *Broadfoot* [1972], a prime source of irradiance data in the 2100- to 2900-Å spectral region. Our results, however, are in close agreement with the 1977 data obtained by G. Rottman (private communication, 1979) near solar minimum using the same rocket instrument.

The Broadfoot data set is one of the few directly calibrated measurements of solar irradiance in the 2100- to 2900-Å region, and his data are in agreement with the data of others taken at longer wavelengths ($\lambda > 2700$ Å) [cf. *Heath and Thekaekara*, 1977]. A possible explanation for the difference between our data and the data of Broadfoot, and for Broadfoot's agreement with others above 2700 Å, could be the presence of a large amount of scattered light in his spectrometer. A scattering 'residue' in Broadfoot's reduced data would produce high fluxes near 2100 Å, where the solar flux is relatively lower than that near 2900 Å. Our data are in closer agreement with Broadfoot at 2550 Å than at 2100 Å, in agreement with this hypothesis. Replicas of the grating used by Broadfoot (B and L 35-53-06-17) have been studied in our laboratory; all the replicas exhibit large ghosts and high scattering [*Rottman*, 1980]. Further, *Delaboudinière et al.* [1978] report that Broadfoot's data are too high below 2300 Å. The ±10% error bars on Broadfoot's data are certainly overly optimistic.

The agreement between the data of June 5, 1979, and the 1977 data of Rottman above 2100 Å (G. Rottman, private communication, 1979) leaves little doubt that the discrepancy with Broadfoot's data is an instrument problem and not an intrinsic variation in the solar flux above 2000 Å as suggested by *Heath* [1973]. It should be of particular interest to aeronomers to note that our data are not compatible with the results presented by *Heath and Thekaekara* [1977, Figure 8].

The FUV and MUV spectrometers also measured the intensities of several strong emission lines of atomic species. Results are given in Table 3 together with line intensity ratios of this flight to Rottman's average solar minimum values. Variances for the five solar minimum line fluxes ranged from 10 to 40% and will be discussed by G. Rottman (unpublished data, 1980). Direct measurements were possible for all lines except H Ly α 1216 Å. It was necessary to increase the measured peak Ly α flux by a small percentage because the intrinsic width of the Ly α line is wider than the slit width of the FUV spectrometer. The fraction of flux not in our band pass was determined by measuring the ratio of the area of a 'standard' Ly α profile as given by *Vidal-Madjar* [1975] to the area of the profile not in our band pass. The correction was only a few percent.

This integrated Ly α line flux is 1.4 times higher than the average of Rottman's five Ly α values measured during solar minimum (R_z between 20 and 64). Although Rottman's results indicate that the relation of R_z to Ly α flux is very weak, it is of interest to use recent empirical relationships to see if the Ly α flux increase can be explained solely by active regions. Using the relation between sunspot number and fractional plage area given by *Cook et al.* [1980], we determine the fractional flat disk area covered by plages as 13%. *Basri et al.* [1979] report an average active region to average quiet sun enhancement at Ly α of a factor of 4.6. (This ratio is the integrated profile contrast; the Ly α profile contrast at 1200 Å is greater

TABLE 2 Solar Irradiance in Units of 10^{10} ph cm^{-2} s^{-1} Å^{-1} Averaged in 10-Å Intervals at 1 AU

	10-Å Intervals									
	00–10	10–20	20–30	30–40	40–50	50–60	60–70	70–80	80–90	90–100
1200	0.218	5.11	0.048	0.037	0.029	0.032	0.042	0.028	0.025	0.027
1300	0.147	0.039	0.031	0.231	0.029	0.054	0.043	0.044	0.048	0.125
1400	0.103	0.064	0.067	0.074	0.076	0.082	0.100	0.116	0.123	0.118
1500	0.131	0.134	0.177	0.205	0.300	0.289	0.237	0.236	0.228	0.228
1600	0.259	0.289	0.334	0.421	0.457	0.673	0.525	0.608	0.603	0.807
1700	1.04	1.10	1.15	1.22	1.15	1.25	1.38	1.43	1.61	1.59
1800	1.94	2.26	2.16	2.24	2.05	2.13	2.28	2.75	2.68	3.03
1900	2.97	3.29	3.49	2.95	3.22	4.18	4.23	4.79	4.72	4.77
2000	5.17	5.85	6.19	6.71	7.67	8.21	8.51	9.86	11.1	16.0
2100	20.8	26.1	24.3	23.9	33.0	26.7	27.0	27.5	37.8	39.9
2200	40.2	31.1	42.3	56.0	49.9	43.9	32.5	33.3	46.9	40.3
2300	47.1	40.7	47.5	37.5	34.3	47.4	44.5	43.0	36.3	40.4
2400	35.9	53.8	64.6	58.4	57.1	45.5	44.7	52.0	41.0	51.8
2500	54.0	39.5	37.7	49.9	49.1	47.0				

TABLE 3. Absolute Line Fluxes

Species	Wavelength, Å	Flux, ph cm^{-2} s^{-1}	Ratio Solar Maximum / Solar Minimum
Si III	1206.53	1.7E10	3.8
H Ly	1215.68	4.36E11	1.4*
N V	1238.82	7.1E8	...
N V	1242.80	5.3E8	...
Si II	1260.42	4.9E8	...
Si II	1264.74	9.2E8	...
O I	1302.17	4.7E9	2.3
O I	1304.86		
O I	1306.03	9.3E9	2.1
C II	1334.53		
C II	1335.66	2.2E10	2.9
O I	1355.60	9.6E8	1.9
Si IV	1393.76	7.4E9	2.9
Si IV	1402.77	3.3E9	2.8
Si II	1526.71	4.20E9	...
C IV	1548.20	1.6E10	2.4
C IV	1550.77	6.9E9	...
C I	1561†	6.8E9	1.5
He II	1640.33‡	9.4E9	...
C I	1657†	2.7E10	2.0
Si II	1808.01	1.3E10	...
Si II	1816.93, 1817.45	2.6E10	0.9

Solar maximum is derived from present data. Solar minimum is the average of five solar minimum flights (Rottman, unpublished data, 1980): five-flight line flux variance range 10–40%.

*Rottman (unpublished data, 1980) Ly α fluxes at solar minimum: 3.08E11, 2.02E11, 2.20E11, 3.7E11, 4.28E11 ph cm^{-2} s^{-1}.

†Multiplet.

‡Fe II blend?

than 4.6 [see *Basri et al.* [1979]. Accordingly, 11% of the solar disk would be predicted to be covered with active regions at the time of the June 5 flight in order to reproduce our measured ratio of Ly α flux to the average of the five Rottman Ly α flux measurements made at solar minimum. Although there is apparent agreement between the two predictions, the large variation in Rottman's solar minimum Ly α values at low R_z (see Table 3) and the average Ly α solar maximum/minimum ratio of approximately 2.5 (requiring a 45% fractional plage area), measured by *Hinteregger* [1979], indicate that this agreement may be largely fortuitous. Furthermore, *Vernazza and Reeves* [1978] report average active region to average quiet sun enhancement factors for the other strong emission lines in the wavelength range 1206-1335 Å which require active region areas varying from 37% to 302% of the area of the solar disk to explain the measured solar maximum to solar minimum intensity ratios. Therefore although there is strong evidence that the variability from solar minimum to solar maximum 1200-1800 Å cannot be explained simply by an increase in the number of active regions on the disk as suggested by *Cook et al.* [1980], further measurements over the cycle will be required to resolve this question unambiguously.

CONCLUSIONS AND FUTURE WORK

We conclude that there is a significant variability in the solar spectral irradiances from solar minimum to solar maximum at wavelengths short of 1800 Å with the change varying from less than the ±15% measurement error at 2000 Å to a factor of 2.5 near 1200 Å. We find no evidence for solar variability exceeding our measurement error of approximately ±15% above 2000 Å. We also conclude that the irradiance values of *Broadfoot* [1972] from 2100 to 2550 Å should be reduced by 35% ± 15%. We find good agreement with previous results in the 1800- to 2100-Å region. Many emission line intensities at wavelengths below ~1850 Å are also significantly enhanced over the solar minimum values.

Future flights will extend the wavelength coverage of the MUV instrument to 3200 Å to connect with ground-based calibrations. We also plan to fly two additional spectrometers to cover the 300- to 1200-Å and 40- to 300-Å wavelength ranges, respectively.

Acknowledgments. We wish to express our appreciation to both the NASA and Lockheed teams at White Sands Missile Range responsible for the successful flight. We wish to thank W. G. Fastie for use of the CTE calibration system at Johns Hopkins University, and S. G. Tilford and R. K. Seals, Jr., for their support of the irradiance investigation under NASA grant NSG 7559 to the University of Colorado. The irradiance instruments were launched on a solar rocket supported at the Laboratory for Atmospheric and Space Physics by NASA grant NSG 5178.

The Editor thanks J. W. Cook and H. E. Hinteregger for their assistance in evaluating this paper.

REFERENCES

Basri, G., J. Linsky, J. Bartoe, G. Brueckner, and M. Van Hoosier, Lyman alpha rocket spectra and models of the quiet and active solar chromosphere based on partial redistribution diagnostics, *Astrophys. J., 230*, 924, 1979.

Broadfoot, L., The solar spectrum 2100-3200 Å, *Astrophys. J., 173*, 681, 1972.

Brueckner, G., J. Bartoe, O. Kjeldseth-Moe, and M. VanHoosier, Absolute solar ultraviolet intensities and their variations with solar activity, I, The wavelength region 1750-2100 Å, *Astrophys. J., 209*, 935, 1976.

Canfield, L., R. Johnston, and R. Madden, NBS detector standards for the far ultraviolet, *Appl. Opt. 12*, 1611, 1973.

Cook, J., G. Brueckner, and M. VanHoosier, Variability of the solar flux in the far ultraviolet 1175-2100 Å, *J. Geophys. Res., 85*, 2257, 1980.

Delaboudiniere, J., R. Donnelly, H. Hinteregger, G. Schmidtke, and P. Simon, Intercomparison compilation for the Lyman bands of molecular hydrogen, *Tech. Manual Ser. 7*, Comm. on Space Res., Tel-Aviv, Israel, 1978.

Fastie, W., and D. Kerr, Spectroradiometric calibration techniques in the far ultraviolet A stable emission source for the Lyman bands of molecular hydrogen, *Appl. Opt., 14*, 2133, 1975.

Guenther, B., and D. Williams, NBS-SURF calibrations: Use in NASA stratosphere and climate programs, paper presented at the Synchrotron Radiation Instrumentation Conference, Nat. Bur. of Stand., Washington, D. C., June 4, 1979.

Heath, D., Space observations of the variability of the solar irradiance in the near and far ultraviolet, *J. Geophys. Res., 78*, 2779, 1973.

Heath, D., and M. Thekaekara, The solar spectrum between 1200 and 3000 Å, in *The Solar Output and Its Variation*, edited by O. White, University of Colorado Press, Boulder, 1977.

Hinteregger, H., Preliminary results of EUVS experiment on AE-E, paper presented at Symposium on the Study of the Solar Cycle from Space, NASA/Amer. Astron. Soc., Wellesley, Mass., 1979.

Mount, G., G. Yamaski, W. Fowler, and W. Fastie, Compact far ultraviolet emission source with rich spectral emission 1150-3100 Å, *Appl. Opt., 16*, 591, 1977.

Rottman, G., Disc values of the solar ultraviolet flux, 1150-1850 Å, *Eos Trans. AGU, 56*, 1157, 1974.

Rottman, G., OSO-8 high resolution spectrometer, Final Report to NASA, Lab. for Atmos. and Space Phys., Univ. of Colo., Boulder, in press, 1980.

Samain, D. and P. C. Simon, Solar flux determination in the spectral range 150-210 nm, *Solar Phys., 49*, 33, 1976.

Simon, P. C., Nouvelles mesures de l'ultraviolet solaire dans la stratosphere, *Bull. Cl. Sci. Acad. Roy. Belg., 61*, 399, 1975.

Simon, P. C., Irradiation solar flux measurements between 120 and 400 nm, Current position and future needs, *Planet. Space Sci., 26*, 355, 1978.

Vernazza, J., and E. Reeves, Extreme ultraviolet composite spectra of representative solar features, *Astrophys. Jr., 223*, 703, 1978.

Vidal-Madjar, A., Evolution of the solar Lyman alpha flux during four consecutive years, *Solar Phys., 40*, 69, 1975

(Received December 20, 1979,
revised March 4, 1980,
accepted March 27, 1980.)

Reprinted from SPIE Vol. 279—Ultraviolet and Vacuum Ultraviolet Systems

Photon-counting array detectors for space and ground-based studies at ultraviolet and vacuum ultraviolet (VUV) wavelengths

J. Gethyn Timothy
Laboratory for Atmospheric and Space Physics, University of Colorado, Boulder, Colorado 80309
Richard L. Bybee
Ball Aerospace Systems Division, Boulder, Colorado 80306

Abstract

The Multi-Anode Microchannel Arrays (MAMAs) are a family of photoelectric photon-counting array detectors, with formats as large as (256 x 1024)-pixels that can be operated in a windowless configuration at vacuum ultraviolet (VUV) and soft x-ray wavelengths or in a sealed configuration at ultraviolet and visible wavelengths. In this paper, we describe the construction and modes of operation of (1 x 1024)-pixel and (24 x 1024)-pixel MAMA detector systems that are being built and qualified for use in sounding-rocket spectrometers for solar and stellar observations at wavelengths below 1300 A. We also describe briefly the performance characteristics of the MAMA detectors at ultraviolet and VUV wavelengths.

Introduction

The feasibility of studying astrophysical plasmas at ultraviolet and VUV wavelengths using space instruments, and the need to study the characteristics of high-temperature plasmas in fusion test reactors, such as Tokamaks, have created requirements for imaging photoelectric array detectors that can be operated both in a sealed configuration at ultraviolet wavelengths longer than 1100 A, and in an open configuration at shorter wavelengths. The Multi-Anode Microchannel Arrays (MAMAs) are a family of photoelectric photon-counting array detectors that have been developed specifically to meet these needs. These detectors combine the high sensitivity and photometric stability of a conventional channel electron multiplier (CEM) with a high resolution imaging capability. Furthermore, these detectors are rugged and simple to use and have been fully qualified for sounding-rocket flights.

In this paper, we describe the construction and modes of operation of (1 x 1024)-pixel and (24 x 1024)-pixel MAMA detector systems that are being built and qualified for use in sounding-rocket spectrometers for solar and stellar observations at wavelengths below 1300 A. We also summarize the parameters of the MAMA detectors which are of importance for space applications and describe briefly their performance characteristics at ultraviolet and VUV wavelengths.

Multi-Anode Microchannel Arrays

Two types of Multi-Anode Microchannel Array (MAMA) detector systems have been developed, as shown in the schematics in Figure 1. The discrete-anode MAMA detector[1] (Figure 1a) consists of a tube assembly (sealed or open) containing an array of metal anodes and a single curved-channel microchannel plate (MCP) with the appropriate photocathode material deposited on the input face. The detector resolution elements (pixels) are defined solely by the physical dimensions of the electrodes in the anode array, which is mounted in proximity focus with the output face of the MCP. The photocathode material defines the spectral range of the detector and the curved-channel MCP provides the high gain and narrow output pulse-height distribution required for pulse-counting operation with a noise level determined solely by the statistics of the photon detection rate. A charge amplifier and discriminator circuit, which issues a logic pulse for each output charge-pulse from the MCP that exceeds a pre-set threshold, is connected to each anode. These pulses are accumulated in a set of counting circuits for a pre-determined exposure time. The number of events recorded in each counting circuit is proportional to the number of photons (or charged particles) incident upon that part of the front face of the MCP that corresponds spatially to the anode location.

Since the number of pixels in a discrete-anode array is limited to about 500 by the currently available connector and electronics technologies, we have developed the coincidence-

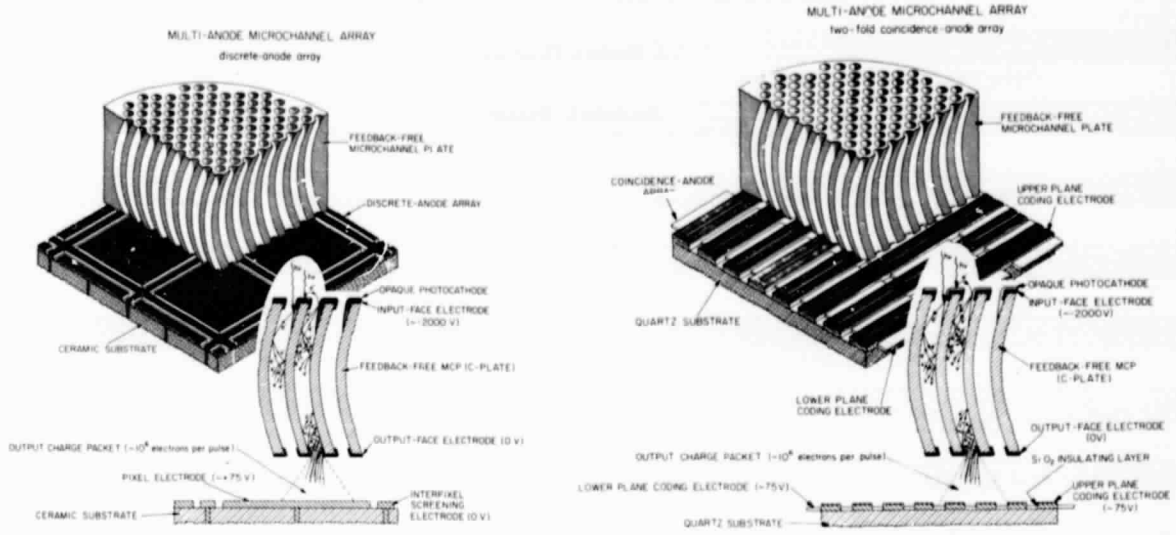

(a) (b)

Figure 1. Multi-Anode Microchannel Arrays
a. Discrete-anode array. b. Coincidence-anode array.

anode MAMA detector[2] which employs two sets of anode electrodes, insulated from each other but exposed to the output face of the MCP, as shown in Figure 1b. In the coincidence-anode MAMA detector the spatial location of an event is determined by the simultaneous detection of a charge-pulse on the two sets of anode electrodes. Using this technique, a total of a x b pixels can be uniquely defined using only a total of a + b sets of anode electrodes. A (1 x 1024)-pixel array, for example, which has a total of 32 x 32 pixels, requires only 32 + 32 sets of anode electrodes. A charge amplifier and discriminator circuit, which issues a logic pulse for each output charge-pulse from the MCP that exceeds a pre-set threshold, is connected to each set of anode electrodes. Any valid combination of coincident logic pulses is decoded to determine the spatial location of an event. The number of events occurring at each spatial location is stored in the corresponding word of a Random Access Memory (RAM). This decoding and storage process is repeated at a maximum rate determined by the pulse-pair resolution of the electronics. A number of discrete- and coincidence-anode MAMA detectors have been fabricated or are under development at this time. The characteristics of these detectors are listed in Table 1 and details of the configurations of these different anode arrays may be found in the literature[3,4].

Table 1. Characteristics of Discrete- and Coincidence-Anode MAMA Detectors

Array Type	Tube Model	Pixel Format	Pixel Dimensions $(mm)^2$	Number of Amplifiers	Maximum Count Rate* (counts s^{-1}) Each Pixel	Total Array	Availability
Discrete-Anode	549-162 or 549-169	10 x 10	1.2 x 1.2	100	1.4×10^6	1.4×10^8	Now
	"	1 x 160	8 x 0.100	160	8×10^5	1.3×10^8	Now
Coincidence-Anode	"	1 x 512	8 x 0.025	48	2×10^5	10^6	Now
	"	1 x 1024	6.5 x 0.025	64	1.7×10^5	10^6	Now
	"	16 x 1024	0.380 x 0.025	80	9.7×10^3	10^6	Now
	"	24 x 1024	0.260 x 0.025	88	6.6×10^3	10^6	Now
	"	512 x 512	0.025 x 0.025	96	6.5×10^3	10^6	Now
	"	256 x 1024	0.025 x 0.025	96	6.5×10^3	10^6	Now
	549-172	1024 x 1024	0.028 x 0.028	128	7.8×10^3	10^6	December 1981

*Limits for 10% loss of detection efficiency with MCP providing 10^6 counts mm^{-2} s^{-1} and electronics dead time of 100 ns.

Sounding rocket detector systems

Two coincidence-anode MAMA detector systems, with anode-array formats of 1 x 1024 pixels and 24 x 1024 pixels respectively, are currently being fabricated and tested specifically for use in sounding-rocket spectrometers. The configuration of the anodes in the (1 x 1024)-pixel linear array is shown in the schematic in Figure 2a. The 16-fold positional ambiguity for each of the 32 fine-position anodes is removed by the 32 coarse-position anodes, and a total of 64 amplifier and discriminator circuits is required for the 1024 spatial locations. The (1 x 1024)-pixel anode array, with pixel dimensions of 6.5 mm x 25 microns is shown in Figure 2b.

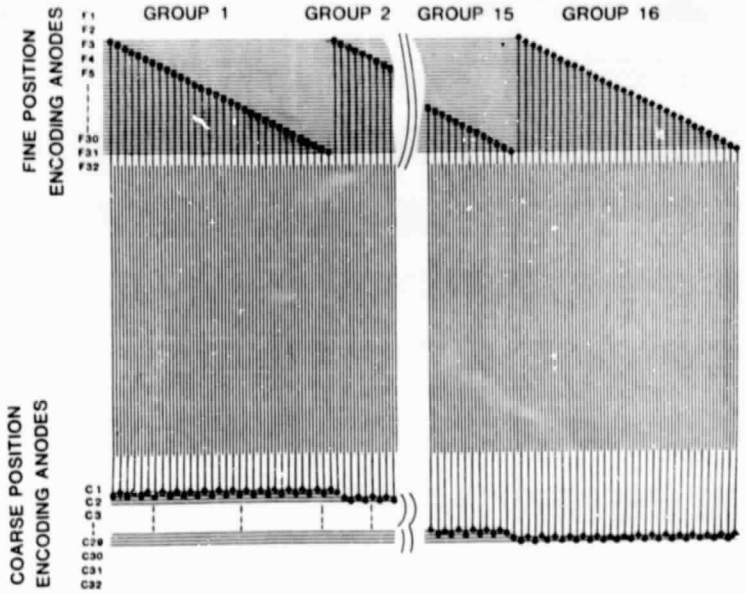

(a)

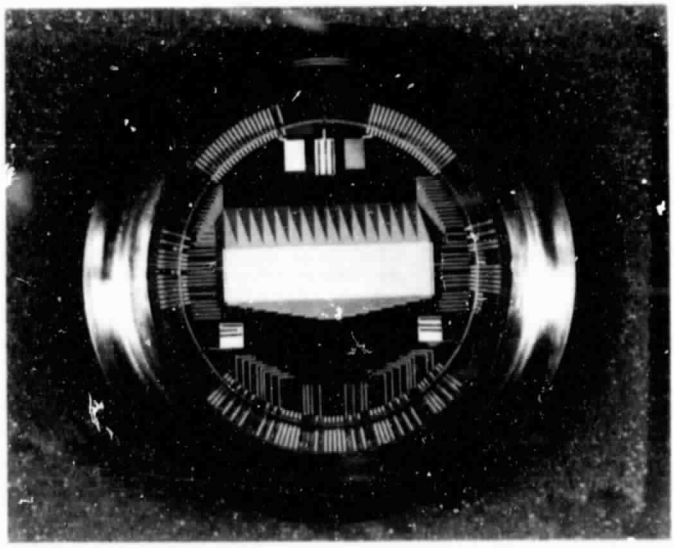

(b)

Figure 2. (1 x 1024)-pixel coincidence-anode array.
a. Anode-array configuration.
b. Anode array with pixel dimensions of 6.5 mm x 25 microns.

Since an exact match between the microchannels in the MCP and the linear electrodes in the anode array cannot be guaranteed, the coincident arrival of pulses on either two or three adjacent anodes is identified and stored as an address in the decoding electronics. Positional information is thus obtained from 2048 pixels (corresponding to a spatial resolution of 12.5 microns in the array). Adjacent two-fold events are then summed to produce the required 25-micron spatial resolution with a high uniformity of response from pixel to pixel. The random coincidence of pulses in different parts of the array is recognized by the electronics as an invalid event and is disregarded. The block diagram of the electronics for the (1 x 1024)-pixel detector system is shown in Figure 3.

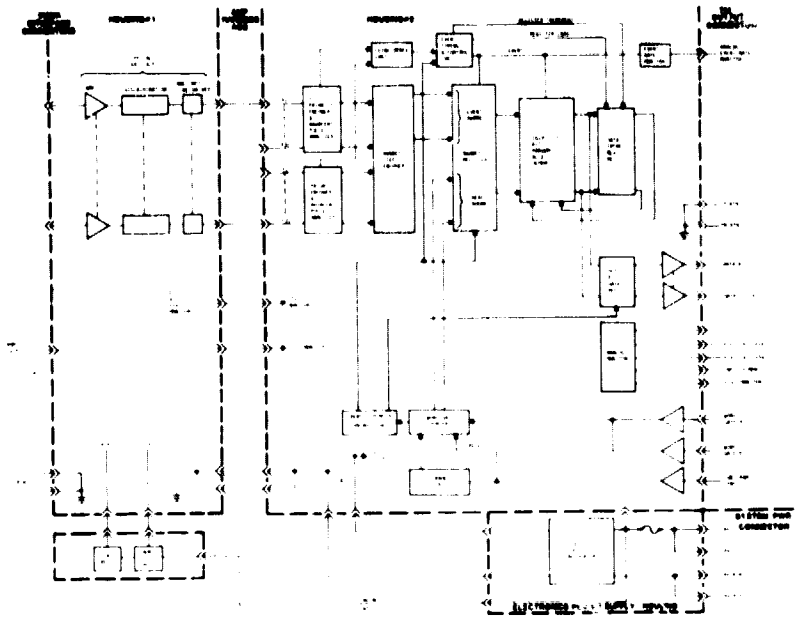

Figure 3. Block diagram of the electronics for the (1 x 1024)-pixel coincidence-anode detector system.

In the (24 x 1024)-pixel coincidence-anode array, an additional set of 24 discrete-anode electrodes is fabricated beneath the upper coincidence-anode electrodes, as shown in the schematic in Figure 1a. The electrodes in the two layers are insulated from each other but exposed to receive the low-energy (~30 V) electrons from the MCP. These multi-layer arrays are fabricated to our specifications by the Raytheon Company[5]. The (24 x 1024)-pixel anode array with pixel dimensions of 260 microns by 25 microns is shown in Figure 4b. The coincident arrival of pulses on two or three vertical anodes and one horizontal anode is used to identify valid events, and a total of 88 amplifier and discriminator circuits is required for the 24,576 spatial locations, as shown in the electronics block diagram in Figure 5.

The open-structure (1 x 1024)-pixel detector has been incorporated in an evacuated VUV spectrometer that is being used to measure the absolute values of the solar spectral irradiances at wavelengths from 250 to 1250 A, and to determine the magnitudes of the variabilities of the spectral irradiances over the solar cycle. As shown in the schematic in Figure 6, the spectrometer employs a 1028-groove mm^{-1} concave diffraction grating, with a radius-of-curvature of 0.25 m, in a conventional normal-incidence mounting. The detector housing is the rear body assembly of the model 549-169 MAMA detector tube, manufactured to our specifications by EMR Photoelectric, Inc.[6]. The 1024-pixel MAMA detector monitors the entire spectrum from 250 to 1250 A with a spectral resolution of approximately 2 A (2 pixels per spectral resolution element) and a temporal resolution during the rocket flight of 2 s. The spectrometer is evacuated prior to launch, opened for observations during the rocket flight, and re-sealed prior to re-entry. Since there are no moving parts in the spectrometer, a hydrocarbon-free, high-vacuum environment is preserved to guarantee the photometric stability of the instrument.

As shown in Figure 7, the electronics are divided into two packages, with the amplifiers, discriminators and line drivers mounted adjacent to the detector assembly, and the address-

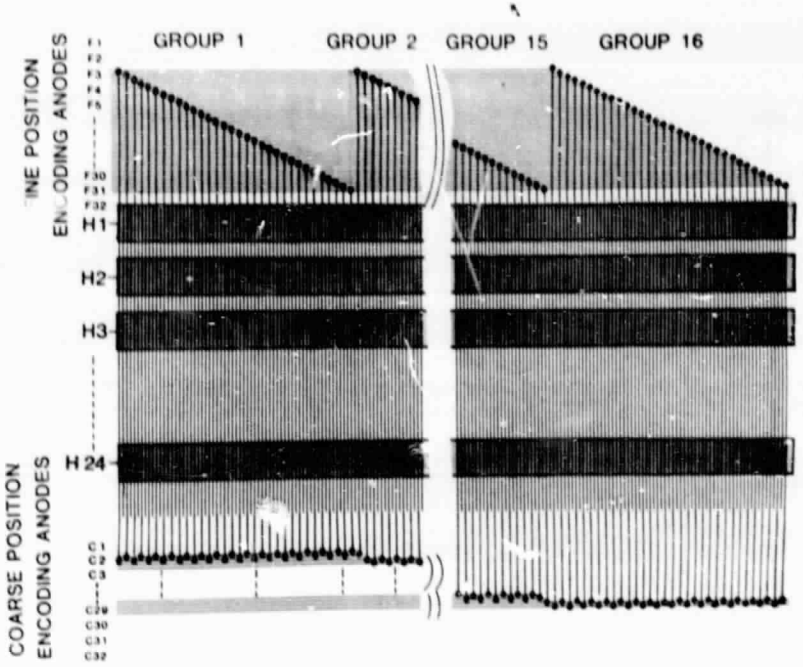

(a)

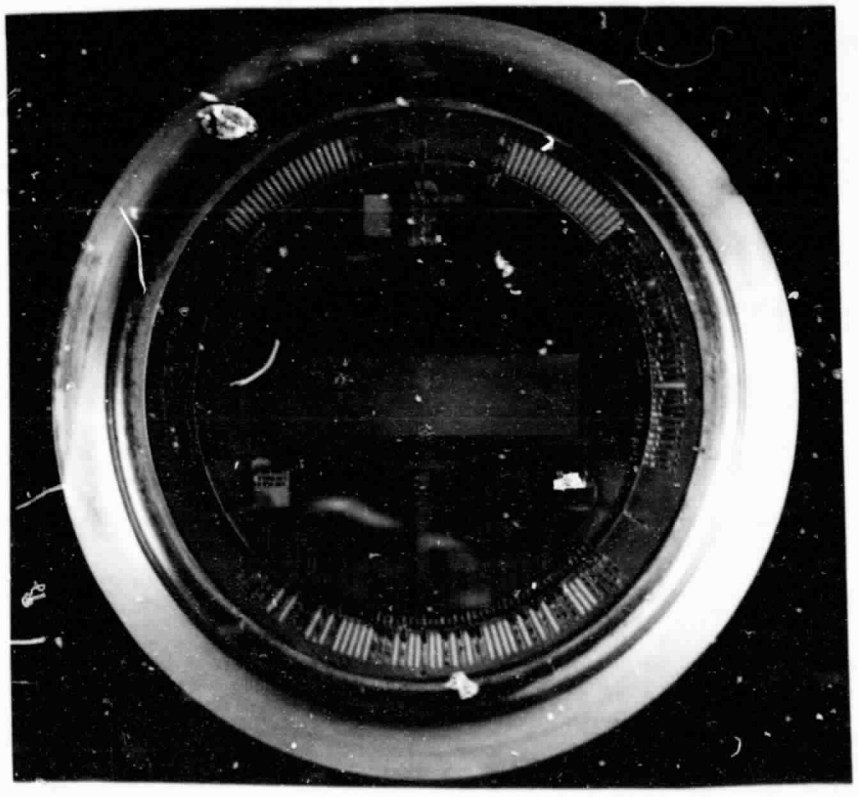

(b)

Figure 4. (24 x 1024)-pixel coincidence-anode array.
a. Anode-array configuration.
b. Anode array with pixel dimensions of 260 microns by 25 microns.

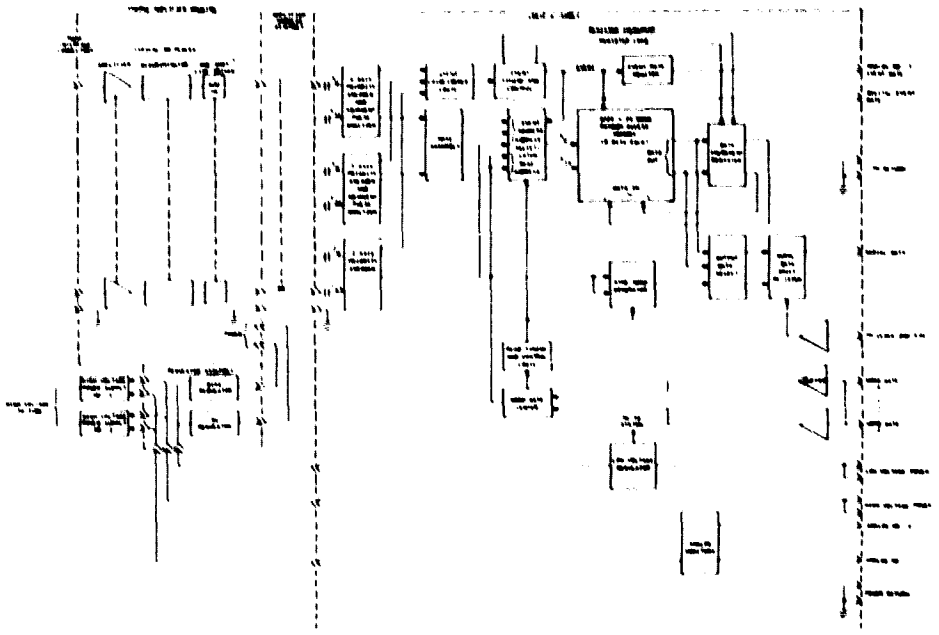

Figure 5. Block diagram of the electronics for the (24 x 1024)-pixel coincidence-anode detector system.

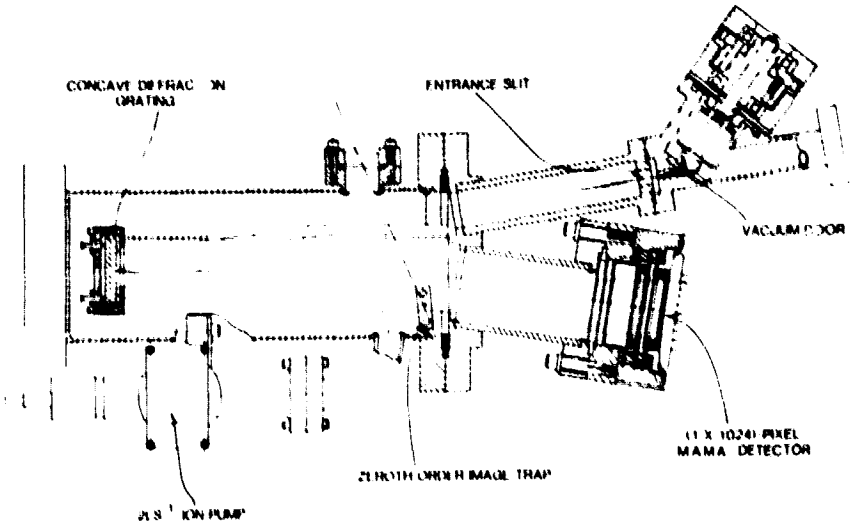

Figure 6. Schematic of evacuated VUV spectrometer with (1 x 1024)-pixel coincidence-anode MAMA detector.

decoding circuits and the 1024 x 10-bit RAM located remotely from the optical instrument. The spectrometer and the detector system have been fully qualified for sounding-rocket flights, and have survived vibration at a level of 20 g rms over the frequency range from 20 to 2000 Hz. The spectrometer is currently undergoing optical alignment and focusing tests in preparation for photometric calibration using the National Bureau of Standards (NBS) SURF II synchrotron-radiation facility.

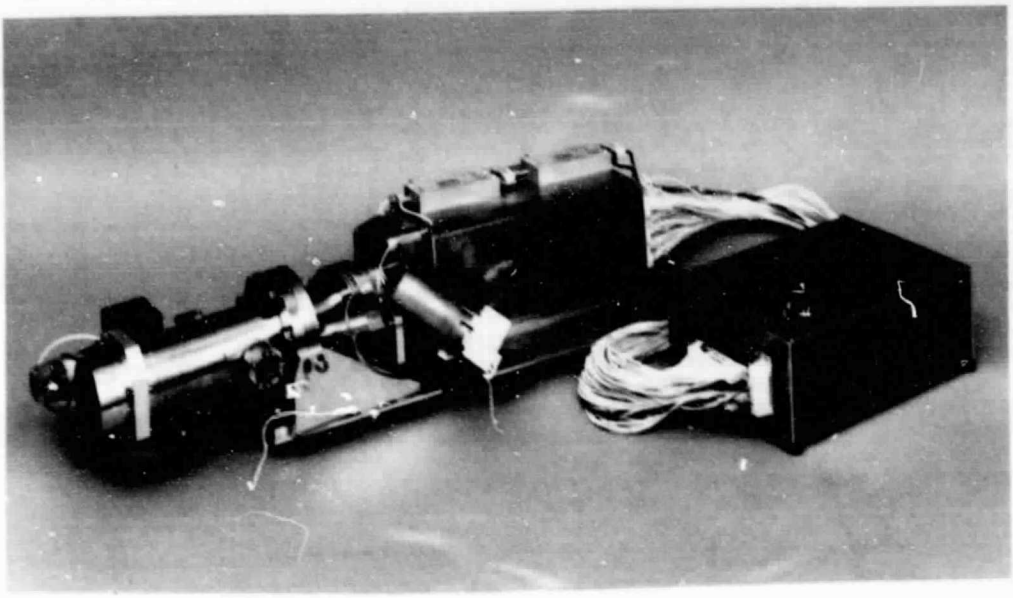

Figure 7. VUV spectrometer and electronics assemblies.

The (24 x 1024)-pixel detector system will be used in an evacuated echelle spectrometer, mounted at the focus of a 40-cm-diameter Cassegrain telescope system with a servo-controlled secondary mirror for image stabilization. This high-spectral-resolution instrument will have numerous and broad applications to a variety of scientific problems, including studies of the interstellar medium, mass loss from OB stars, the nature of Be stars, and coronal emission lines from cool stars. Although it is being prepared for initial flight on a Black Brant sounding rocket, the stellar instrument has been designed, from the outset, for future flights on the Space Shuttle. The 0.5-m focal-length echelle spectrometer will have an initial resolving power ($\lambda/\Delta\lambda$) of 60,000 over the wavelength range from 900 to 1200 A. During the first sounding-rocket flight, the instrument will study several aspects of the interstellar medium, including element abundances, velocity structure, and interstellar extinction. The (24 x 1024)-pixel coincidence-anode detector will be used to record data from eight echelle orders and determine the inter-order scattered light levels simultaneously. Data will be recorded simultaneously over a total spectral range of about 80 A. This open-structure MAMA detector, which has a configuration similar to that employed in the solar VUV spectrometer, will have an opaque CsI photocathode deposited on the front face of the MCP after it is installed in the spectrometer, in order to provide the maximum quantum efficiency at wavelengths between 900 and 1200 A.

The (24 x 1024)-pixel detector system is currently nearing completion and will be under test at the end of March 1981. As the result of the fabrication of the (1 x 1024)-pixel and (24 x 1024)-pixel detector systems, we have developed a general packaging scheme which can be used for any of the discrete- or coincidence-anode MAMA detectors listed in Table 1. The dimensions of the different assemblies are shown in Figure 8. Two assemblies are required for each of the detector systems, except for the (512 x 512)- and (256 x 1024)-pixel coincidence-anode arrays which require an additional memory assembly, as shown in Figure 8c.

Performance characteristics

The performance characteristics of the MAMA detector systems offer a number of significant advantages over alternative photoelectric imaging systems currently under development for space and ground-based studies at ultraviolet and VUV wavelengths. The most important of these characteristics, some of which are mandatory for reliable operation in the vacuum environments encountered in space and in ground-based VUV instrumentation, are:

1) The detector operates at high gain ($>10^6$ electrons pulse^{-1}) in the pulse-counting mode with an applied potential of less than 3 kV. This is a significantly lower voltage than any other comparable image-intensifier system and ensures that the detector can be safely operated in an open-structure configuration under vacuum at pressures of 10^{-5} Torr or lower.

2) No cooling of the detector system is required for pulse-counting operation at ultraviolet and VUV wavelengths.

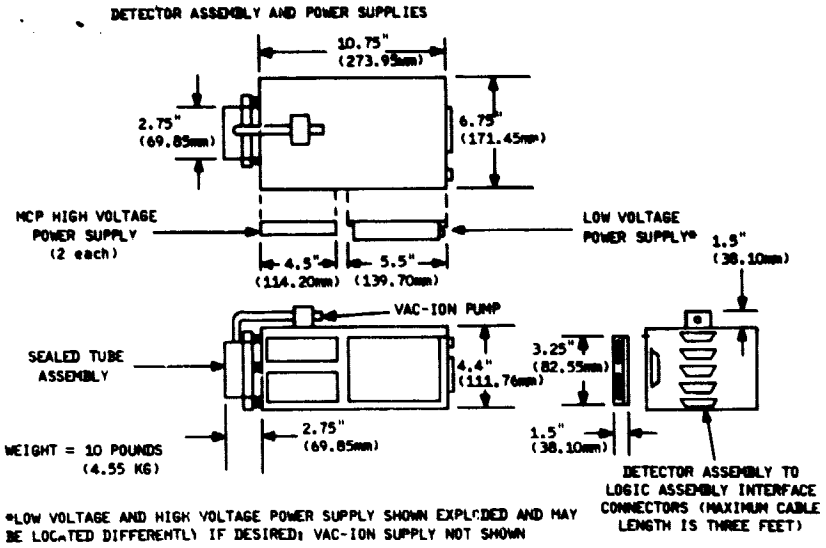

(a)

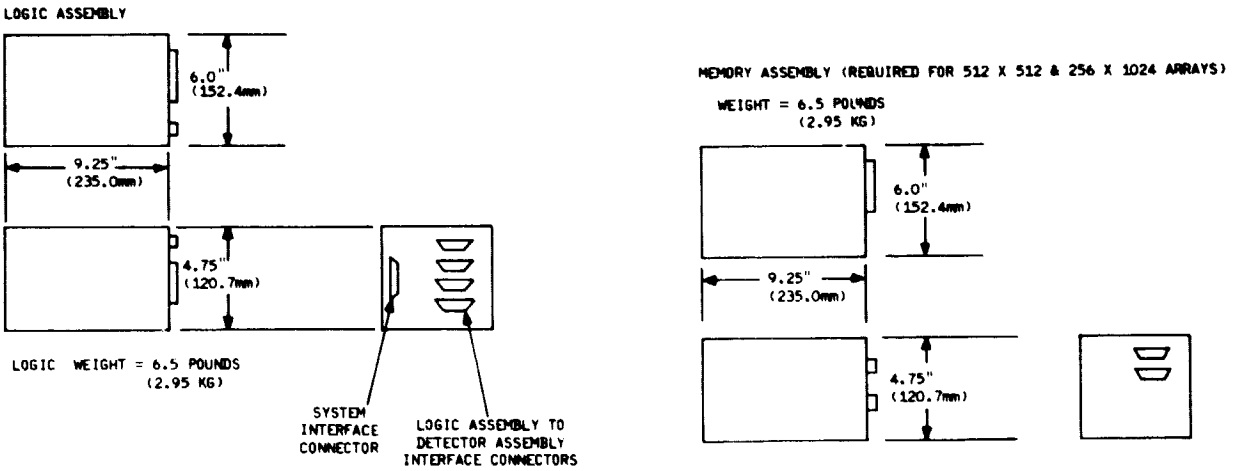

(b) (c)

Figure 8. Schematics of MAMA detector systems for space and ground-based applications.
a. Detector head assembly.
b. Logic assembly.
c. Additional memory assembly (required for (512 x 512)-pixel and (256 x 1024)-pixel detector systems).

3) The total power requirement for a detector system is of the order of 30 W or less, which minimizes the problem of cooling when the electronics are operated under vacuum.

4) The detector system does not use magnetic or electrostatic focusing systems and the spatial accuracy is determined solely by the spacing of the metallic electrodes in the anode array. The resulting image is distortion-free, with a single-pixel resolution that is independent of position in the array or of the signal level.

5) The detector has a high immunity to external magnetic fields of several hundred Gauss.

6) No long-term damage is caused by exposure to high-energy radiation.

7) The detector system has zero readout noise; consequently, the signal-to-noise ratio is determined solely by the photon statistics and by the photocathode dark-count rate.

8) The detector employs a random readout system. The time-of-arrival of an event can be identified with a precision equal to the pulse-pair resolution of the electronics (currently in the range from 700 to 100 ns for the different systems).

9) All data are recorded in a digital format. This greatly facilitates array processing and data manipulation.

10) Data can be selectively read out from any portion of the array. The format can, accordingly, be optimized for a specific observation.

The key to the excellent performance characteristics of the MAMA detectors is the curved-channel MCP. The curved-channel MCPs currently used in the MAMA detector tubes are fabricated by Galileo Electro-Optics Corporation[7] and have C-configuration microchannels (see Figure 9) to inhibit ion-feedback in an identical manner to that employed in a conventional CEM.

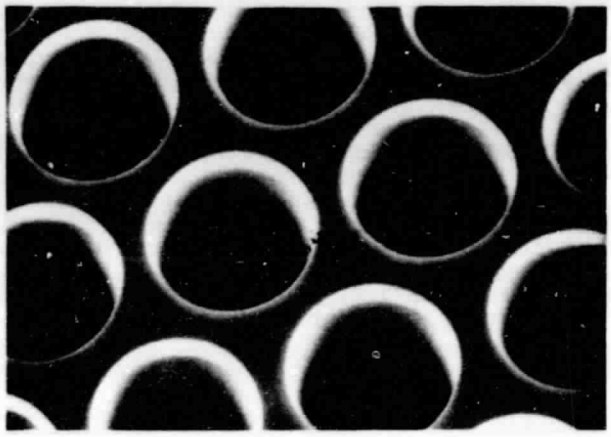

(a)

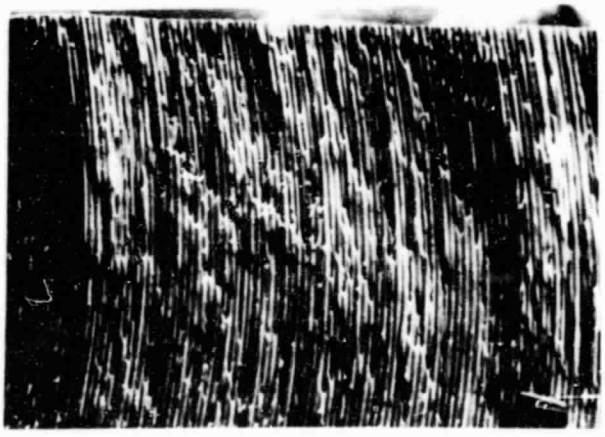

(b)

Figure 9. Curved-channel MCP with 25-micron-diameter channels.
a. Face of plate.
b. Section of plate.

Curved-channel MCPs with both 25-micron-diameter channels on 32-micron centers and 12-micron-diameter channels on 15-micron centers are now available. The length-to-diameter ratios of the channels in the MCPs delivered to date have ranged from 80:1 to 140:1, and

the microchannels have been set at a bias angle of 15° with respect to the input face of the plate. Some units of the curved-channel MCPs have been fabricated with the channel inputs funnelled to increase the open-area ratio to 75-80%. This improves the detection efficiency and facilitates the collection of the high-energy photoelectrons when the MCP is used as a high-spatial-resolution open-structure detector at VUV wavelengths below about 1000 A.

Details of the performance characteristics of the curved-channel MCPs are being presented elsewhere in the literature[8], and we note here only those characteristics which are of fundamental importance for the operation of the MAMA detectors. First, a single curved-channel MCP can be operated stably at high gain in the pulse-counting mode. Accordingly, the loss of spatial resolution caused by charge spreading at the interface of the two MCPs required in a conventional "chevron" MCP detector is eliminated. Second, the amplitude of the output pulse is clipped by the effects of space charge within the channel and the output pulse-height distribution has a quasi-Gaussian form. The resolution of the output pulse-height distribution can therefore be defined as:

$$R = \frac{\Delta G}{\bar{G}} \qquad (1)$$

where ΔG equals the full width at the half-height of the distribution, and $\bar{G}$ equals the modal gain value. Resolutions of the order of 30 to 50% and modal gain values in the range 1 to 3 x 10^6 electrons $pulse^{-1}$ are typically obtained with the curved-channel MCPs.

The narrow pulse-height distribution produces a stable counting plateau in the high-voltage characteristic, and the curved-channel MCP, accordingly, produces a highly stable photometric response without stringent requirements on the stability of the high-voltage supply. In addition, the narrow pulse-height distribution facilitates the rejection of signal capacitatively cross-coupled between adjacent electrodes in the anode array. Accordingly, a highly uniform single-pixel response is obtained with a pixel-to-pixel cross talk of the order of a few percent or less, as shown in Figure 10. Indeed, the imaging quality of the MAMA detectors cannot be measured with our existing test equipment, and the laboratory optical facility is being upgraded in order to determine the limiting performances of the detectors.

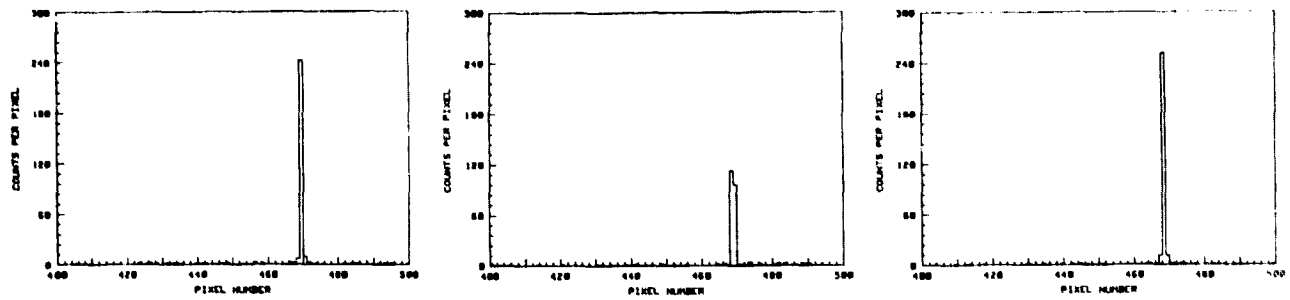

Figure 10. Motion of a slit image in 12.5 micron steps between adjacent 25-micron pixels in the (1 x 1024)-pixel coincidence-anode array.

Finally, when properly conditioned and operated at the correct gain level[8], the curved-channel MCPs have demonstrated intrinsic dark-count rates at room temperature of significantly less than 0.01 counts mm^{-2} s^{-1} and lifetimes in excess of 2.5 x 10^{11} counts mm^{-2}.

The semi-conducting glass of the curved-channel MCP in an open-structure MAMA detector can be used as an efficient photocathode at VUV wavelengths below about 1400 A. Because of the high work function of the glass, the bare MCP is highly insensitive to wavelengths longer than about 2000 A. This greatly facilitates the rejection of long wavelength scattered radiation for studies at VUV wavelengths. In order to enhance the VUV sensitivity an opaque MgF_2 photocathode can be deposited on the front face of the MCP. For ultraviolet applications, an opaque CsI or an opaque Cs_2Te photocathode can be deposited on the front face of the MCP. The response of the MAMA detector can accordingly be effectively tailored to the wavelength range of interest. The characteristics of the photocathode materials utilized to date at ultraviolet and VUV wavelengths are summarized in Table 2.

Table 2. Ultraviolet and VUV photocathode materials for MAMA detectors

Material	Wavelength Range (Å)	Peak Quantum Efficiency (%)	Dark Count Rate (count $mm^{-2}s^{-1}$)
Bare MCP	1-1400	>15 at 600 A	<0.01
MgF_2	1-1000	>25 at 300 A	<0.01
CsI (G)	~1000-1800	>40 at 1216 A	<0.1
Cs_2Te (F)	1200-3200	>10 at 2000 A	<0.2

Full details of the performance characteristics of the detector systems will be presented in the literature at the end of the evaluation program later this year.

Acknowledgements

We wish to acknowledge the assistance that we are continuing to receive from the following individuals with the fabrication of the MAMA detectors: G. Lorman at Ball Aerospace Systems Division with the construction and test of the electronics, P. Graves and P. Henkel at Galileo Electro-Optics Corporation with the fabrication of the curved-channel MCPs, J. Roderick and N. Stamates of EMR Photoelectric with the tube fabrication and photocathode processing, and E. Culver, F. Cheriff and P. Ouellette at the Raytheon Company with the fabrication of the anode arrays. We gratefully acknowledge the unstinting support of Drs. J. Rosendhal, N. Roman and E. Weiler of NASA Headquarters. We thank Dr. T.P. Snow, Jr. of LASP for permission to describe his high-resolution stellar spectrometer.

The MAMA detector-development program is supported by NASA grant NSG 7459. Fabrication of the (1 x 1024)-pixel and (24 x 1024)-pixel detector systems is supported by NASA grants NSG 7559 and NSG 5303 respectively.

References

1. Timothy, J.G. and R.L. Bybee, U.S. Patent No. 4,086,486, 1978.
2. Timothy, J.G. and R.L. Bybee, U.S. Patent No. 4,070,578 1978.
3. Timothy, J.G. and R.L. Bybee, "Multi-Anode Microchannel Array Detectors for Space Shuttle Imaging Applications", S.P.I.E. Shuttle Pointing of Electro-Optical Experiments 265, 93 (1981).
4. Timothy, J.G., G.H. Mount, and R.L. Bybee, "Multi-Anode Microchannel Arrays", IEEE Trans. Nucl. Sci., NS-28, in press (1981).
5. Raytheon Company, Equipment Development Laboratories, Sudbury, MA 01776.
6. EMR Photoelectric Inc., Princeton, NJ 08540.
7. Galileo Electro-Optics Corporation, Sturbridge, MA 01518.
8. Timothy, J.G., "Curved-channel MCPs", Rev. Sci. Instrum., submitted (1981).